NACA RM L56C14

NACA

RESEARCH MEMORANDUM

EFFECT OF LEADING-EDGE DROOP ON THE AERODYNAMIC AND LOADING CHARACTERISTICS OF A 4-PERCENT-THICK UNSWEPT-WING—FUSELAGE COMBINATION AT TRANSONIC SPEEDS

By James W. Schmeer

Langley Aeronautical Laboratory
Langley Field, Va.

NATIONAL ADVISORY COMMITTEE FOR AERONAUTICS

WASHINGTON

May 23, 1956
Declassified October 28, 1960

NATIONAL ADVISORY COMMITTEE FOR AERONAUTICS

RESEARCH MEMORANDUM

EFFECT OF LEADING-EDGE DROOP ON THE AERODYNAMIC AND LOADING CHARACTERISTICS OF A 4-PERCENT-THICK UNSWEPT-WING—FUSELAGE COMBINATION AT TRANSONIC SPEEDS

By James W. Schmeer

SUMMARY

An investigation was conducted in the Langley 16-foot transonic tunnel to determine the effects of leading-edge droop on the aerodynamic and loading characteristics of an unswept wing with a taper ratio of 0.5, an aspect ratio of 4, and NACA 65A004 airfoil sections parallel to the plane of symmetry. The leading edge of the wing was drooped both 6° and 10° about the 17-percent-chord line, full span. Force, moment, and pressure measurements were obtained at Mach numbers from 0.60 to 1.05 and angles of attack, depending on Mach number, from approximately 0° to 16°. The Reynolds number, based on the mean aerodynamic chord, varied from 4.6×10^6 to 6.3×10^6.

The results indicate that, below a Mach number of 0.94, leading-edge droop delayed the onset of leading-edge separation and moved the main wing-compression shock rearward. The maximum lift-drag ratio of the basic wing at a Mach number of 0.60 was increased by 41 percent with 6° leading-edge deflection and by 71 percent with 10° deflection. These gains in lift-drag ratio decreased rapidly with increasing speed and both 6° and 10° deflection reduced the maximum lift-drag ratio above Mach numbers of about 0.85 and 0.78, respectively.

Leading-edge deflection had small effect on the spanwise location of the center of load. The maximum normal load on the wing leading edge (as indicated at two spanwise stations) increased with increasing deflection at a Mach number of 0.60, but with increasing Mach number to about 0.90 and above, the undeflected leading edge carried the higher loads. At low angles of attack, the longitudinal location of the center of load was shifted considerably rearward by leading-edge droop, especially at the higher Mach numbers.

INTRODUCTION

Although the effects of leading-edge droop on the aerodynamic and loading characteristics of swept wings at high subsonic and transonic speeds have been investigated (refs. 1 to 4), little information is available concerning the effects of droop on the characteristics of unswept wings in this speed range. Furthermore, the results of an investigation using a small-scale two-dimensional model (ref. 5) has evoked interest in leading-edge droop as a means of reducing the large pressure pulsations associated with leading-edge flow separation on thin unswept wings. Accordingly, then, the present investigation employing a thin unswept wing with leading-edge droop was conducted in the Langley 16-foot transonic tunnel with a twofold purpose: first, to determine the effects of droop on the steady-state aerodynamic and loading characteristics and, second, to evaluate the effects on the fluctuating loads on a three-dimensional wing. The results of the steady-state aerodynamic and loads investigation are presented in this paper.

The basic wing of this investigation has zero sweep of the 0.50-chord line, a taper ratio of 0.5, an aspect ratio of 4, and NACA 65A004 airfoil sections parallel to the plane of symmetry. The leading edge of the wing was drooped about the 0.17-chord line, full span.

Data were obtained with the leading edge deflected both 6° and 10° through a Mach number range of 0.60 to 1.05 and angles of attack, depending on Mach number, from about 0° to 16°. The Reynolds number based on the mean aerodynamic chord varied from 4.6×10^6 to 6.3×10^6. The data for the basic (undrooped) wing, presented in reference 6, are included herein for comparison purposes. Also included are some ink-flow pictures illustrating the flow on the upper surface of the basic wing and on the wing with 6° leading-edge droop.

SYMBOLS

b	wing span
b'	span of wing panels from 15.9-percent-semispan stations to tips, 57.51 in.
c	local wing chord
c_f	leading-edge chord, 0.17c
c'	mean aerodynamic chord

$\bar{c}$ average wing chord

C_{BM} wing-panel bending-moment coefficient,

$$\frac{4\left(\text{Bending moment of wing panel outboard of 15.9-percent-semispan station}\right)}{qS'b'}$$

C_D drag coefficient, $\frac{\text{Drag}}{qS}$

C_L lift coefficient, $\frac{\text{Lift}}{qS}$

C_m pitching-moment coefficient, $\frac{\text{Pitching moment about } c'/4}{qSc'}$

c_n section normal-force coefficient, $\int_0^{1.0} \left(P_l - P_u\right) d\frac{x}{c}$

$c_n \frac{c}{\bar{c}}$ section normal-load coefficient

c_{n_f} section normal-force coefficient for forward 17 percent of wing, $\int_0^{1.0} \left(P_l - P_u\right) d\frac{x}{c_f}$

c_h section hinge-moment coefficient about 0.17c, $\int_0^{1.0} \left(P_l - P_u\right)\left(1.0 - \frac{x}{c_f}\right) d\frac{x}{c_f}$

C_N model normal-force coefficient, $\frac{\text{Model normal force}}{qS}$

C_N' estimated normal-force coefficient of wing panel outboard of 15.9-percent-semispan station, $0.815 C_N \frac{S}{S'}$

$\left(L/D\right)_{max}$ maximum lift-drag ratio

M free-stream Mach number

P	pressure coefficient, $\frac{p - p_\infty}{q}$
p	local static pressure
P_b	base pressure coefficient, $\frac{p_b - p_\infty}{q}$
p_b	static pressure at base of fuselage
P_{cr}	critical pressure coefficient
p_∞	free-stream static pressure
q	free-stream dynamic pressure
R	Reynolds number based on c'
S	wing area
S'	wing-panel area outboard of 15.9-percent-semispan station, 6.482 sq ft
x	longitudinal distance measured from wing leading edge at any given spanwise station
y	lateral distance measured perpendicular to plane of symmetry
$\bar{y}$	lateral distance from 15.9-percent-semispan station to wing-panel center of loading
$\frac{\bar{y}}{b'/2}$	spanwise center of load parameter, $C_{BM}/C_{N'}$
ΔC_D	total drag coefficient minus drag coefficient for basic wing configuration at zero lift
$\frac{d\Delta C_D}{dC_L^2}$	drag-due-to-lift parameter, average value from $C_L \approx 0.1$ to 0.4
α	model angle of attack (fuselage reference line), deg
ϕ	meridian angle from top of fuselage (looking forward), deg

Subscripts:

u	upper
l	lower

MODEL AND APPARATUS

Model

The steel wing was mounted on the fuselage in a midwing position and had no geometric incidence, twist, or dihedral. Leading-edge droop was obtained by cutting the wing at the 17-percent-chord line and inserting one of two sets of steel splines which were preset to give 6° and 10° deflections. The downward deflection of the leading edge caused a gap on the upper surface; this gap was filled and faired so as to minimize the fairly abrupt change in curvature. The fuselage consists of a cylindrical body of revolution, an ogive nose, and a slightly boat-tailed afterbody. A photograph of the model is shown in figure 1 and the geometric details, including a table of fuselage coordinates, are given in figure 2.

Instrumentation

The overall forces and moments on the model were measured by means of a six-component internal strain-gage balance. In addition, the wing-panel bending moments were obtained from a calibrated strain-gage installation mounted at the 15.9-percent-semispan station on the left wing (fig. 2).

Chordwise pressure distributions on the wing were obtained from pressure orifices located at three spanwise stations. At the innermost station, the orifices were located on the fuselage about 1/16 inch from the basic wing surface. Thus, when the leading edge was deflected, the orifices for the forward 17 percent at this station were no longer properly located with respect to the wing surfaces and were disregarded. Fuselage pressure measurements were obtained from pressure orifices at two radial stations at any given axial position. The wing and fuselage pressure-orifice locations are given in figure 2.

The model base pressures were measured at two orifices mounted flush with the internal surface of the fuselage about 2 inches from the fuselage base.

The tests were conducted in the Langley 16-foot transonic tunnel which has been described in reference 7.

TESTS

Simultaneous measurements of the model forces, moments, and pressures were obtained for the Mach number and angle-of-attack range given in the following table:

Mach number	Approximate angle-of-attack range, deg
0.60	0.3 to 16.1
.80	.3 to 16.4
.85	.3 to 16.6
.90	.3 to 16.9
.94	.3 to 13.0
.98	.3 to 13.0
1.00	.3 to 13.0
1.03	.3 to 10.8
1.05	.3 to 10.8

The variation with Mach number of the test Reynolds number (based on wing mean aerodynamic chord) is given in figure 3.

In order to facilitate comparison of the pressure data for the wing with deflected leading edges with that for the basic wing (ref. 6), an attempt was made to duplicate the angles of attack at each Mach number. In general, the angles of attack were repeated within 0.1°, with slightly greater deviations occurring at the higher angles of attack.

As an aid to visualizing the effects of leading-edge deflection on the flow pattern, some ink-flow pictures were obtained for the basic wing and the wing with 6° leading-edge droop. The ink-flow technique consisted simply of emitting a free-flowing dark-colored liquid from four orifices near the leading edge of the wing and photographing the resulting flow patterns. Both still pictures and motion pictures were obtained at representative Mach numbers through an angle-of-attack range from 0° to an upper limit imposed by the sting support system. Further discussion of this technique may be found in references 4 and 8.

REDUCTION OF DATA AND ACCURACY

The forces and moments were reduced to coefficient form based on the geometry of the basic wing. In general, the total wing geometry was used; however, several coefficients were based on the geometry of the wing panel

outboard of the 15.9-percent-semispan station, namely: wing-panel bending-moment coefficient, wing-panel normal-force coefficient, and lateral center-of-load coefficient. In addition, the section hinge-moment coefficient about 0.17c and the section normal-force coefficient for the forward 17 percent of the wing were based on the chord of the drooped leading edge.

The lift and drag coefficients have been adjusted to a condition of free-stream static pressure at the base of the fuselage; base pressure coefficients for the three configurations are presented in figure 4. No other corrections have been applied to the force and moment coefficients for the effects of sting interference or tunnel boundary interference. These effects are believed to be small (for example, see ref. 9) and furthermore, for a given set of test conditions, to remain nearly constant for the basic wing and the wing with deflected leading edges; therefore, the comparisons made herein should be valid regardless of the magnitude of interference effects.

The accuracy of the basic force, moment, and pressure coefficients is believed to be within the following limits:

C_L	± 0.01
C_D -	
At low lift coefficients	± 0.001
At high lift coefficients	± 0.003
C_m	± 0.003
P	± 0.002

RESULTS

Comparisons of wing and fuselage pressure-coefficient distributions for the basic wing and the wing with 6° and 10° deflected leading edge are presented in figures 5 and 6. The coefficients of lift, drag, pitching moment, and wing-panel bending moment are compared in figures 7 to 10. Summary drag and lift-drag characteristics are presented in figures 11 to 14. The effects of leading-edge droop on the center-of-load location and on the loading characteristics are presented in figures 15 to 19. Ink-flow pictures presented in figure 20 illustrate the flow pattern on the upper surface of the basic wing and the wing with 6° leading-edge droop at representative Mach numbers and angles of attack.

DISCUSSION

Aerodynamic Characteristics

Flow characteristics.- Inasmuch as the general flow characteristics of the basic wing have been discussed in reference 6, the following discussion will be limited to significant differences attributable to leading-edge droop and the relative effects of the two deflection angles. The results of the present tests indicate a somewhat natural division of the effects of leading-edge droop into three Mach number regions. First, the effects at a Mach number of 0.60 are restricted to a delay in leading-edge separation and are probably representative of the subcritical speed range. Second, the effects at Mach numbers of approximately 0.80 to 0.90 are closely associated with changes in the location of the main compression shock on the wing, as well as leading-edge separation. Third, the effects of droop above a Mach number of about 0.94 are not significant.

The pressure-coefficient distribution at a Mach number of 0.60, figure 5(a), shows leading-edge separation on the basic wing at an angle of attack of 9.0° whereas both the 6° and 10° deflected leading edges maintain high negative pressure peaks and good pressure recovery at this angle of attack. With increasing angle of attack, starting on the inboard sections, separation occurs first on the 6° drooped leading edge and then at somewhat higher angles of attack on the 10° drooped leading edge. At $\alpha = 16.1°$, extensive separation exists on the wings with drooped leading edges and except for a small area near the leading edge on the outboard sections, the distributions are practically identical to those of the basic wing.

As was the case at a Mach number of 0.60, leading-edge droop delays leading-edge separation in the Mach number range of approximately 0.80 to 0.90. This delay in separation, shown in figure 5(b) at a Mach number of 0.80 (see $\alpha = 9.3°$ and 13.4°) can also be seen by comparing the ink-flow pictures for the basic wing and the wing with 6° deflection at angles of attack of about 9.2° and 13.4° (figs. 20(a) and 20(b)). Similarly, the pressure-coefficient distributions and ink-flow pictures at the higher angles of attack for a Mach number of 0.85 (figs. 5(c), 20(c), and 20(d)) illustrate the delay in leading-edge separation.

The effects of leading-edge droop on separation have been shown to be similar for subcritical speeds up to Mach numbers of about 0.90. However, in the higher part of this speed range (M = 0.80 to 0.90), extensive areas of supersonic velocities exist on the upper surface of the wing and an additional large effect of leading-edge droop is evident. This effect consists of a flat, highly negative pressure distribution beginning at the drooped leading-edge hinge line (0.17c) and extending rearward to the main wing shock wave. This region of high-velocity flow is due to expansion around the fairly abrupt change in curvature of the upper surface and is

similar to the region of high-velocity flow which starts at the leading edge of the basic wing and also terminates at the main wing shock. This main wing shock, then, occurs further rearward on the wing with deflected leading edge as can be seen, for example, in the pressure-coefficient distribution and ink-flow pictures at a Mach number of 0.80 and an angle of attack of 5° (figs. 5(b), 20(a), and 20(b)). Generally, the level of this flat pressure distribution is more negative for the 10° deflected leading edge as compared with the 6° deflection and the main shock wave is more rearward, although at a Mach number of 0.90 the differences decrease, especially at the higher angles of attack.

At Mach numbers of 0.94 and above, the pressure distributions (figs. 5(e) to 5(h)) show the effects of leading-edge droop to be small (except, of course, for the usual reversal of pressures on the leading edge at low angles of attack). At these speeds, the main wing shock has reached the vicinity of the trailing edge. Thus, the primary disturbances on the wing surface are two fairly weak oblique shock waves (ref. 6), one originating in the vicinity of the fuselage-wing leading-edge juncture and the other at the wing tip; both of these shocks appear to be relatively unaffected by leading-edge droop, especially at moderate and high angles of attack. The ink-flow pictures at $M = 0.94$ (figs. 20(g) and 20(f)) indicate the similarity of the flow patterns for the basic wing and the wing with 6° leading-edge droop. At Mach numbers of 0.98 and 1.00, the flow patterns for the basic wing (fig. 19(h)) are essentially identical to those for the wing with 6° droop, so the latter have been omitted.

The effects of leading-edge deflection on the body pressures ($\phi = 0°$ and 180°) were generally small except whenever droop delayed extensive separation on the inboard sections of the wing. At this condition, the effects of droop were carried over the upper surface of the body and separation was delayed, similar to the effect on the inboard sections of the wing. For example, see the pressure-coefficient distributions at $M = 0.85$ and $\alpha = 11.4°$, figure 5(c) (wing) and figure 6(a) (fuselage).

Lift characteristics.- The lift curves of figure 7 show that both 6° and 10° leading-edge droop increased the lift coefficient at high angles of attack in the Mach number range of 0.60 to 0.90; 10° deflection provided the largest gains, amounting to about 0.2 in C_L at $M = 0.90$. At a Mach number of 0.60, the increased lift is due to the delay in leading-edge separation as shown in figure 5(a). With increasing Mach number up to about 0.90, the area of high-velocity flow between the hinge line of the drooped leading edge and the main wing shock wave which occurred further rearward for the wing with deflected leading edge (see figs. 5(b), 5(c), and 5(d)), also increases the lift at the higher angles of attack. At a Mach number of 0.94 and above, there was no indication of extensive separation on the

basic wing and the main wing shock was located near the trailing edge; thus, no improvements were obtained from leading-edge deflection. In fact, due to the loss of lift on the deflected leading edge, C_L was decreased through most of the angle-of-attack range at these speeds.

Drag characteristics.- The drag polars are presented in figure 8 and drag coefficient at constant values of lift coefficient is plotted against Mach number in figure 11. In the latter figure, it can be seen that the penalty in zero-lift drag caused by deflecting the leading edge generally increases with Mach number. Increasing the deflection from 6° to 10° causes larger increases in zero-lift drag than the initial deflection from basic to 6°. At moderate to high values of C_L, both deflections reduce the drag at the lower Mach numbers. With increasing Mach number, increasingly higher values of C_L are required in order to obtain any drag benefits.

The reductions in drag at lifting conditions appear to be due mainly to reduced chord force since the lift-curve slopes were not much affected by droop and thus the drag component of the normal force $\left(1/C_{L_\alpha}\right)$ was not significantly changed. The reduction in chord force at the lower Mach numbers is evident in the pressure-coefficient distributions of figure 5, which show that droop maintained negative leading-edge pressure peaks to higher angles of attack with a resultant better pressure recovery at the trailing edge. The reason for the reduction in chord force at Mach numbers greater than 0.90 for the higher angles of attack is not obvious from the pressure distributions of figure 5, which shows lower negative pressure peaks on the deflected leading edges and nearly identical pressure recovery over the trailing edges. However, the deflected leading edge has greater projected frontal area so that negative pressures on the upper surface (even though of lower value than for the basic) can have a greater thrust component. Similarly, a positive pressure on the lower surface will have a smaller drag component; in fact, the 10° deflected leading edge receives some thrust.

A drag-due-to-lift parameter was obtained from the slopes of ΔC_D plotted against C_L^2. These curves were quite linear at all test Mach numbers through a C_L range from slightly higher than zero up to about 0.4. The results, presented in figure 12, show that, at $M = 0.60$, the 6° deflection decreased the drag-due-to-lift parameter by over 40 percent and the 10° deflection by over 50 percent. At this speed, the drag-due-to-lift parameter for the wing with 10° droop approaches the theoretical minimum for this wing plan form as defined by $1/\pi A$. With increasing Mach number, the reduction due to 6° deflection decreased to about 18 percent at $M = 1.05$ while the reduction due to 10° deflection decreased with speed up to $M = 0.94$ and then increased again to about 45 percent at $M = 1.05$.

The maximum lift-drag ratio of the basic wing at a Mach number of 0.60 was increased by about 41 percent by 6° deflection and by about 71 percent by 10° deflection (fig. 13). However, these benefits decrease rapidly with increasing Mach number and both the 6° and 10° deflections reduce $(L/D)_{max}$ at Mach numbers above 0.85 and 0.78, respectively. Also shown in figure 13 is the increase of C_L for $(L/D)_{max}$ due to leading-edge deflection.

The ratio of L/D for the wing with leading-edge droop to L/D for the basic wing through the lift range is presented in figure 14. As was the case for $(L/D)_{max}$, both 6° and 10° deflections greatly increased L/D at moderate to high lift coefficients at the lower Mach numbers. For example, at $M = 0.60$ and $C_L = 0.5$, 10° droop doubles the value of L/D for the basic wing. With increasing Mach number, however, the benefits again decrease rapidly, with 6° deflection showing slightly better values of L/D than the 10° deflection. Based on L/D considerations, it appears that the deflection of the leading edge should decrease with increasing Mach number. This same conclusion was indicated in reference 10 which showed the effects at high subsonic speeds of a leading-edge flap on a wing of similar plan form but different profile.

Pitching-moment characteristics.- At $M = 0.60$, both leading-edge deflections provide negative pitching moments at zero lift (fig. 9). With increasing Mach numbers up to 0.94, the value of C_m at zero lift becomes increasingly more negative, amounting to as much as -0.07 and -0.09 for 6° and 10° deflections, respectively. The deflected leading edge does not alter the unstable tendencies of the basic wing at the lower Mach numbers, but does delay to higher values of C_L, the strong stabilizing break.

The data of figure 9 also indicate that the tail loads required for trim at values of C_L near cruising at the lower Mach numbers would be less for the wing with deflected leading edge, and thus the drag benefits discussed earlier might be increased. On the other hand, trimming out the large negative moments at the higher Mach numbers would probably incur further drag penalties.

At low angles of attack, the longitudinal location of the center of load is shown in figure 15 to be shifted considerably rearward by leading-edge droop, especially at the higher Mach numbers. However, with increasing angle of attack, this difference becomes negligible.

LOADING CHARACTERISTICS

Wing-Panel Loads

In order to determine the lateral center-of-load location for the wing with drooped leading edges, it was assumed that the wing panel outboard of the bending-moment gages carried a constant proportion of the total load through the Mach number and angle-of-attack range. This assumption was found to be essentially correct for the basic wing in reference 6 where the ratio of wing-panel normal force to total normal force was calculated to be 0.815. A comparison at two spanwise stations of the normal-load parameter $c_n \frac{c}{\bar{c}}$ for the basic wing and the wing with deflected leading edges (fig. 16) indicates that, except for some erratic differences above stall conditions, the same proportion of total load could be assumed for the wing with drooped leading edges. The lateral center-of-load position was then determined from the values of bending moment (fig. 10) measured at 0.159b/2 and the estimated wing-panel normal force. It can be seen in figure 17 that except for lower Mach numbers at low values of C_N', the maximum difference in center-of-load location due to leading-edge droop was about 2 or 3 percent.

Additional Load on the Wing Leading Edge

In figure 18, the effect of leading-edge droop on the section normal-force coefficient for the forward 17 percent of the wing is shown at two semispan stations for three representative Mach numbers. The maximum positive increment in normal load on the leading edge due to deflection occurred at a Mach number of 0.60, as indicated in figure 18(a). At this speed, the maximum leading-edge loads increased with increasing deflection. With increasing speed, the positive increment of c_{n_f} due to deflection decreased and at a Mach number of 0.90 and above, the leading edge of the basic wing carried the highest positive normal loads for the angle-of-attack range tested (figs. 18(b) and 18(c)). Also shown in figures 18(b) and 18(c) are the large increases in negative normal loads due to leading-edge deflection at low values of C_N and high Mach numbers.

The section hinge-moment coefficients about 0.17c, shown in figure 19, follow closely the same trends as the section normal-force coefficients for the leading edge.

CONCLUSIONS

The results of an investigation of the effects of leading-edge droop on the transonic aerodynamic and loading characteristics of an unswept wing with a taper ratio of 0.5, an aspect ratio of 4, and NACA 65A004 airfoil sections parallel to the plane of symmetry lead to the following conclusions:

1. Leading-edge droop delayed the onset of leading-edge separation to higher angles of attack at Mach numbers below 0.94 and caused the main wing compression shock wave to seek a more rearward location at Mach numbers from 0.80 to 0.94; 10° deflection had larger effects than 6° deflection.

2. Leading-edge droop increased the maximum lift coefficient at Mach numbers up to about 0.90; 10° deflection provided slightly greater increases than 6° deflection.

3. Leading-edge droop decreased drag at moderate to high values of lift coefficient with the maximum reduction occurring at a Mach number of 0.60 and decreasing with increasing Mach number; 10° deflection was more effective at the lower Mach numbers and 6° deflection at the higher Mach numbers.

4. Leading-edge droop increased the maximum lift-drag ratio at a Mach number of 0.60, amounting to about a 41-percent and 71-percent increase over that of the basic wing for the 6° and 10° deflection, respectively. The advantage of droop decreased rapidly with increasing Mach number and became zero at Mach numbers of approximately 0.85 and 0.78 for the 6° and 10° deflections, respectively.

5. Leading-edge droop had small effect on the spanwise location of the center of load.

6. The maximum normal load on the wing leading edge (forward 17 percent) increased with deflection at a Mach number of 0.60, but with an increase in Mach number to about 0.90 and above, the leading edge of the basic wing carried the highest positive normal loads.

7. At low angles of attack, the longitudinal location of the center of load was shifted considerably rearward by leading-edge droop, especially at the higher Mach numbers.

Langley Aeronautical Laboratory,
National Advisory Committee for Aeronautics,
Langley Field, Va., February 23, 1956.

REFERENCES

1. Spreeman, Kenneth P., and Alford, William J., Jr.: Investigation of the Effects of Leading-Edge Flaps on the Aerodynamic Characteristics in Pitch at Mach Numbers From 0.40 to 0.93 of a Wing-Fuselage Configuration With a 45° Sweptback Wing of Aspect Ratio 4. NACA RM L53G13, 1953.

2. Spreeman, Kenneth P., and Alford, William J., Jr.: Small-Scale Transonic Investigation of the Effects of Full-Span and Partial-Span Leading-Edge Flaps on the Aerodynamic Characteristics of a 50° 38' Sweptback Wing of Aspect Ratio 2.98. NACA RM L52E12, 1952.

3. Schmeer, James W., and Cooper, J. Lawrence: Effects of Increasing Reynolds Number From 2×10^6 to 6×10^6 on the Aerodynamic Characteristics at Transonic Speeds of a 45° Swept Wing With 6° Leading-Edge Droop. NACA RM L54L10, 1954.

4. Schmeer, James W.: The Effects of Leading-Edge Droop Upon the Pressure Distribution and Aerodynamic Loading Characteristics of a 45° Sweptback Wing at Transonic Speeds. NACA RM L55I16, 1955.

5. Humphreys, Milton D., and Kent, John D.: The Effects of Camber and Leading-Edge-Flap Deflection on the Pressure Pulsations on Thin Rigid Airfoils at Transonic Speeds. NACA RM L52G22, 1952.

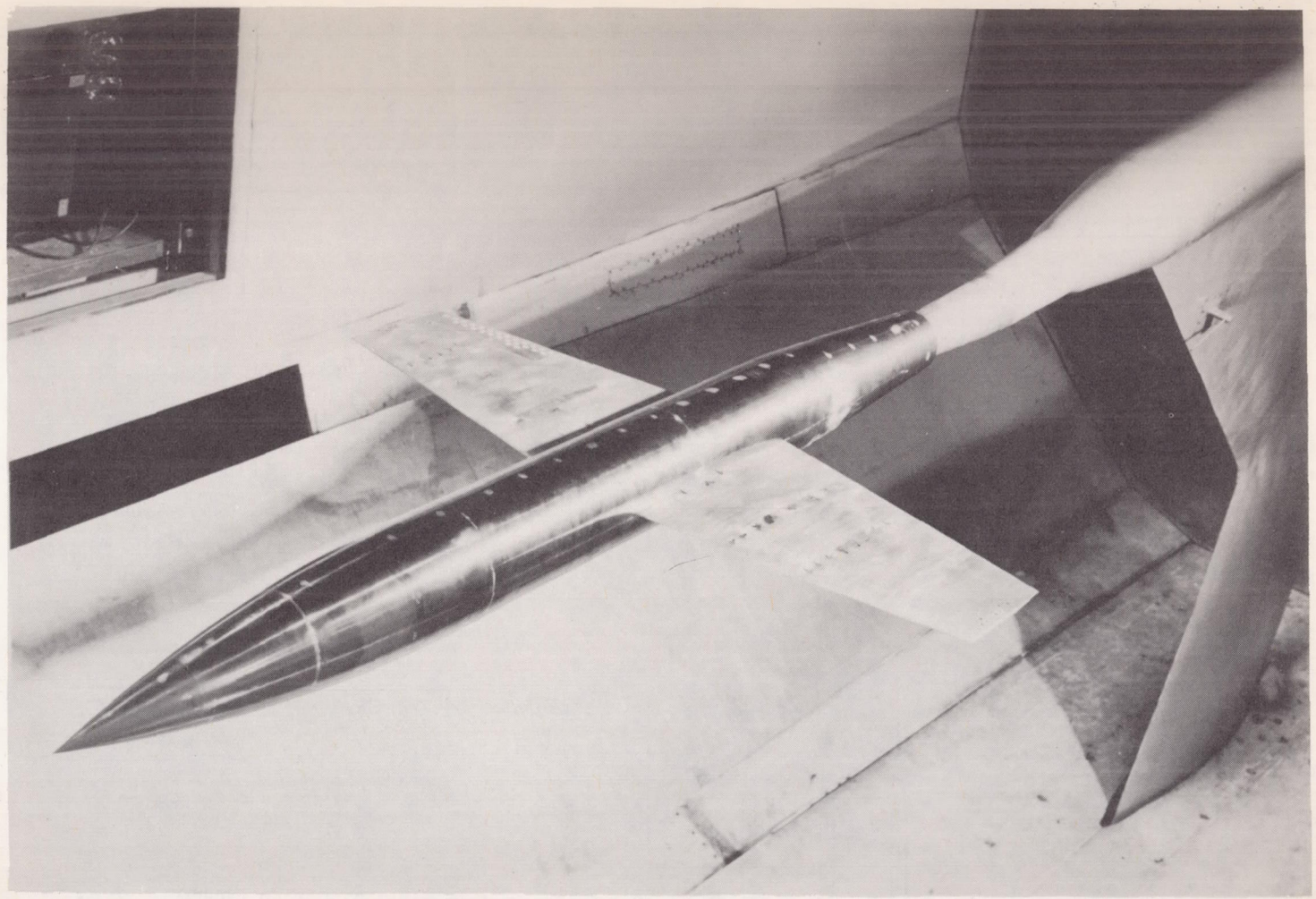
6. Hieser, Gerald, Henderson, James H., and Swihart, John M.: Transonic Aerodynamic and Loads Characteristics of a 4-Percent-Thick Unswept-Wing—Fuselage Combination. NACA RM L54B24, 1954.

7. Ward, Vernon G., Whitcomb, Charles F., and Pearson, Merwin D.: Air-Flow and Power Characteristics of the Langley 16-Foot Transonic Tunnel With Slotted Test Section. NACA RM L52E01, 1952.

8. Runckel, Jack F., and Schmeer, James W.: The Aerodynamic Characteristics at Transonic Speeds of a Model With a 45° Sweptback Wing, Including the Effects of Leading-Edge Slats and a Low Horizontal Tail. NACA RM L53J08, 1954.

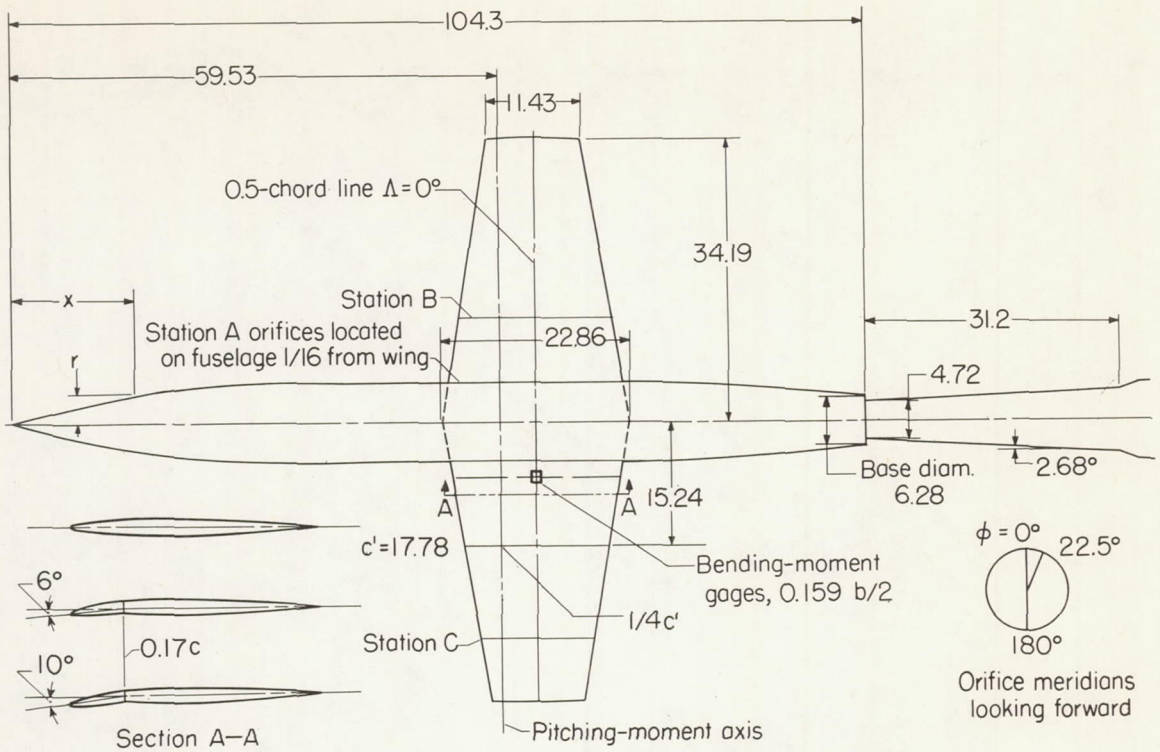
9. Whitcomb, Charles F., and Osborne, Robert S.: An Experimental Investigation of Boundary Interference on Force and Moment Characteristics of Lifting Models in the Langley 16- and 8-Foot Transonic Tunnels. NACA RM L52L29, 1953.

10. Johnson, Ben H., Jr., and Reed, Verlin D.: Investigation of a Thin Wing of Aspect Ratio 4 in the Ames 12-Foot Pressure Wind Tunnel. IV - The Effects of a Constant-Chord Leading-Edge Flap at High Subsonic Speeds. NACA RM A8K19, 1949.



L-80814

Figure 1.- The model with basic wings in the Langley 16-foot transonic tunnel.



Fuselage ordinates			
x	r	x	r
0.000	0.000	24.000	4.396
0.500	0.144	26.000	4.536
1.000	.286	28.000	4.643
1.500	.426	30.000	4.716
2.000	.564	32.000	4.755
3.000	.832	33.333	4.763
4.000	1.091	78.582	4.763
5.000	1.341	79.000	4.757
6.000	1.582	79.250	4.752
7.000	1.812	79.500	4.746
8.000	2.035	80.000	4.728
9.000	2.249	80.500	4.708
10.000	2.454	81.000	4.685
10.500	2.551	81.916	4.639
11.000	2.649	83.500	4.557
11.625	2.766	85.250	4.458
12.000	2.834	87.000	4.345
14.000	3.182	88.000	4.278
16.000	3.493	89.000	4.209
18.000	3.770	90.965	4.067
19.000	3.896	97.362	3.624
20.000	4.014	104.300	3.143
22.000	4.223		

Wing data	
Aspect ratio	4.0
Taper ratio	0.5
Wing area	8.165 sq ft
Airfoil section	65A004

Wing orifice locations		
Spanwise station location, percent semispan		
A	13.9	
B	37.5	
C	77.7	
Location of each station percent chord		
0	25.00	65.00
1.25	30.0	70.00
2.50	35.00	75.00
5.00	40.00	80.00
7.50	45.00	85.00
10.00	50.00	90.00
15.00	55.00	95.00
20.00	60.00	

Fuselage orifice locations	
Percent length	Angle from top looking forward
2.00	0°, 180°
4.00	
8.00	
12.00	
20.00	
28.00	
34.00	
38.00	
42.00	
46.00	
50.00	
54.00	
58.00	
62.00	
66.00	
70.00	
74.00	
78.00	
82.00	22.5°, 180°
86.00	
90.00	
94.00	
98.00	

Figure 2.- Geometric details of model. All dimensions are in inches.

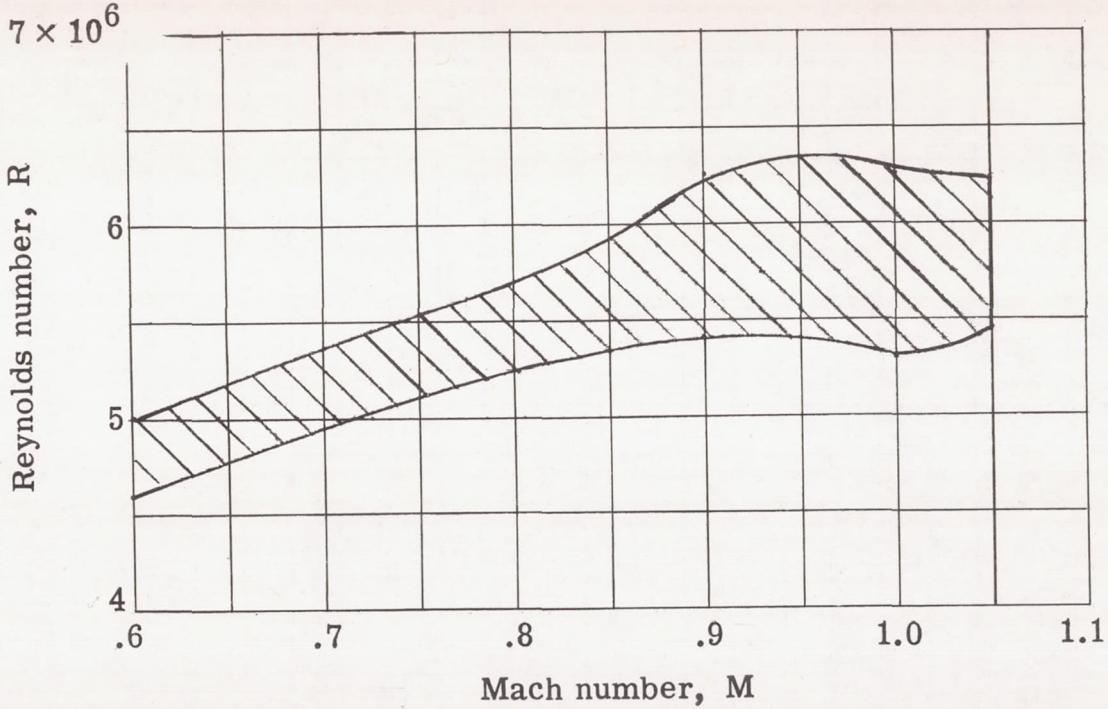


Figure 3.- Variation of Reynolds number with Mach number.

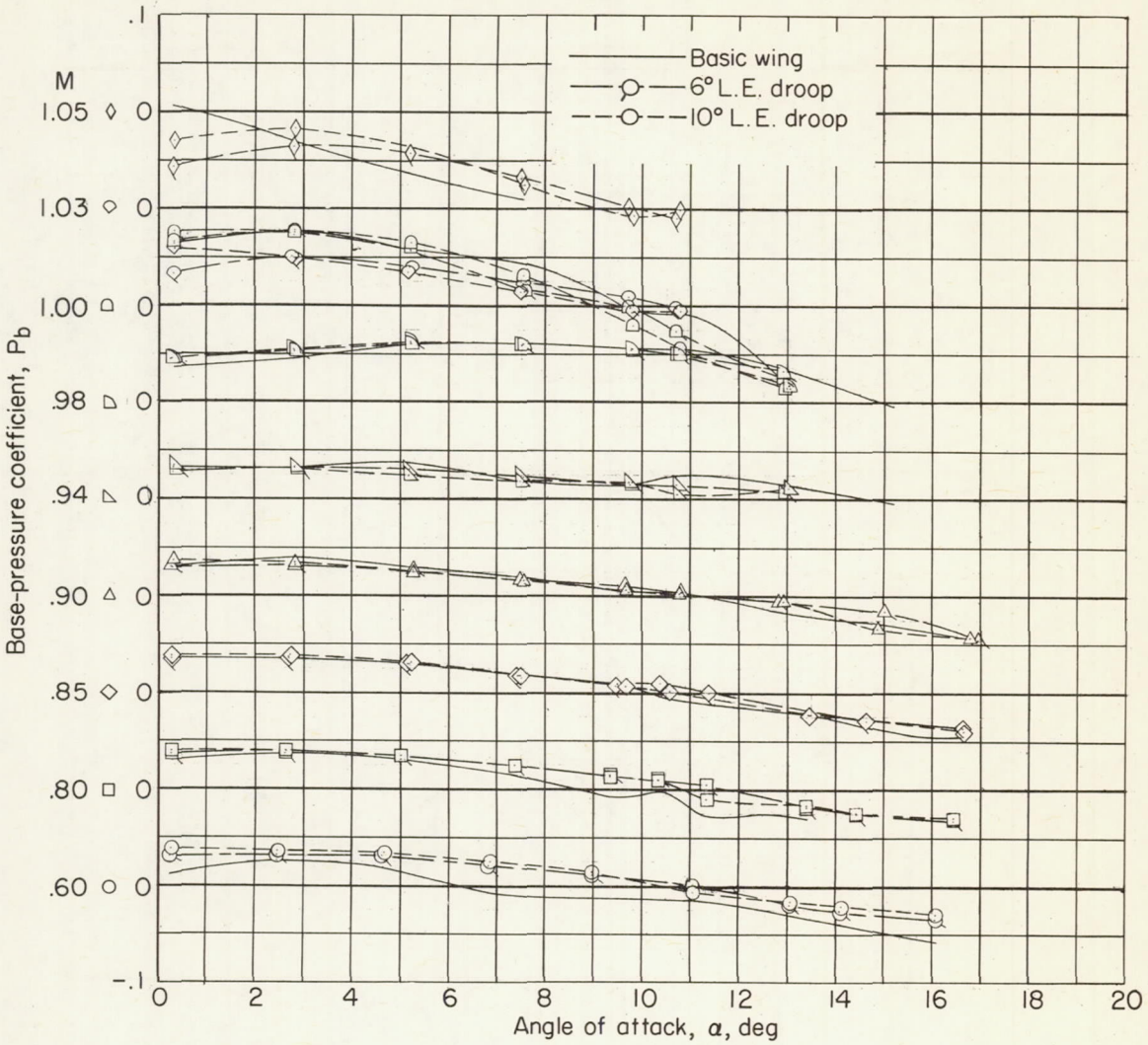
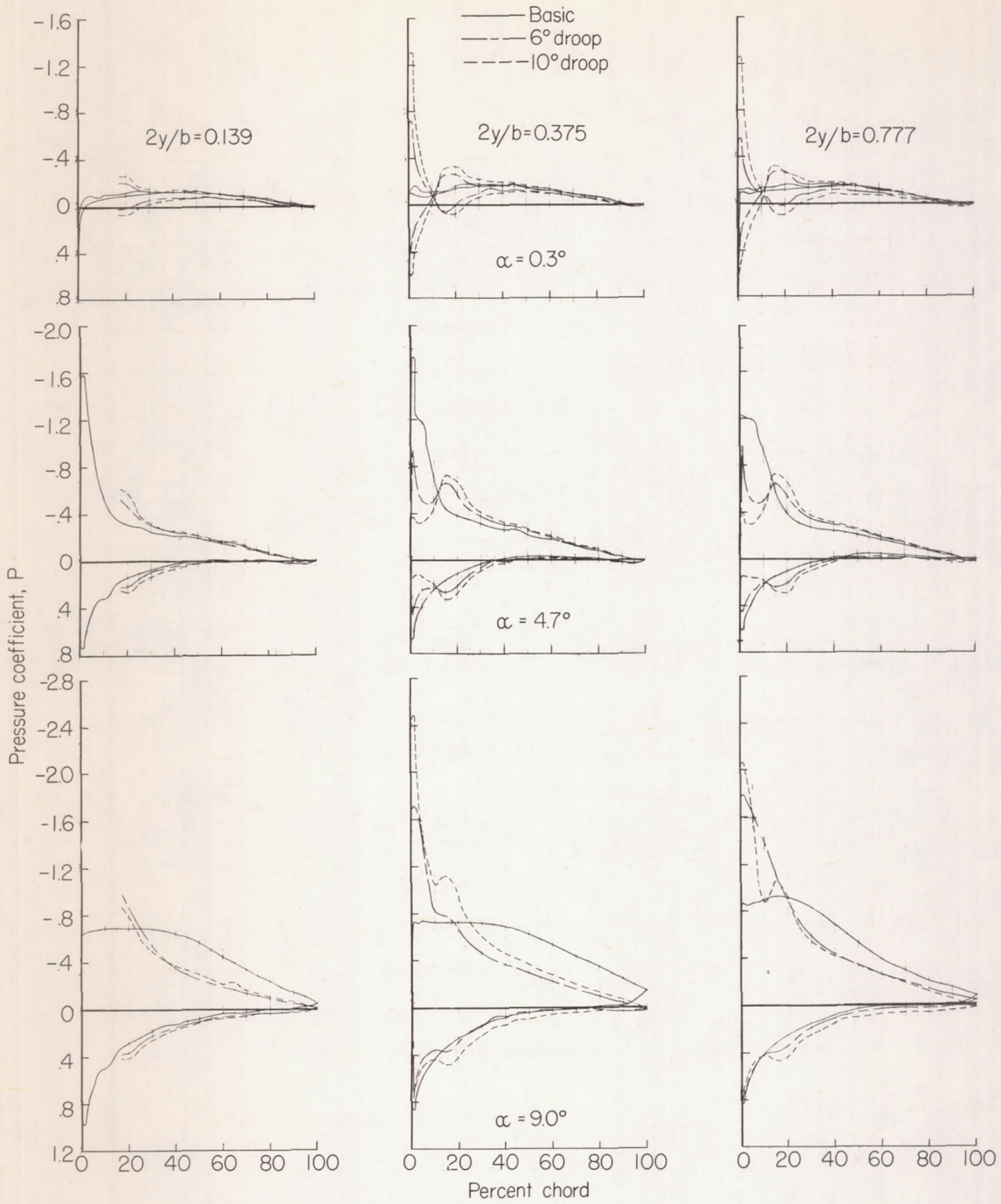
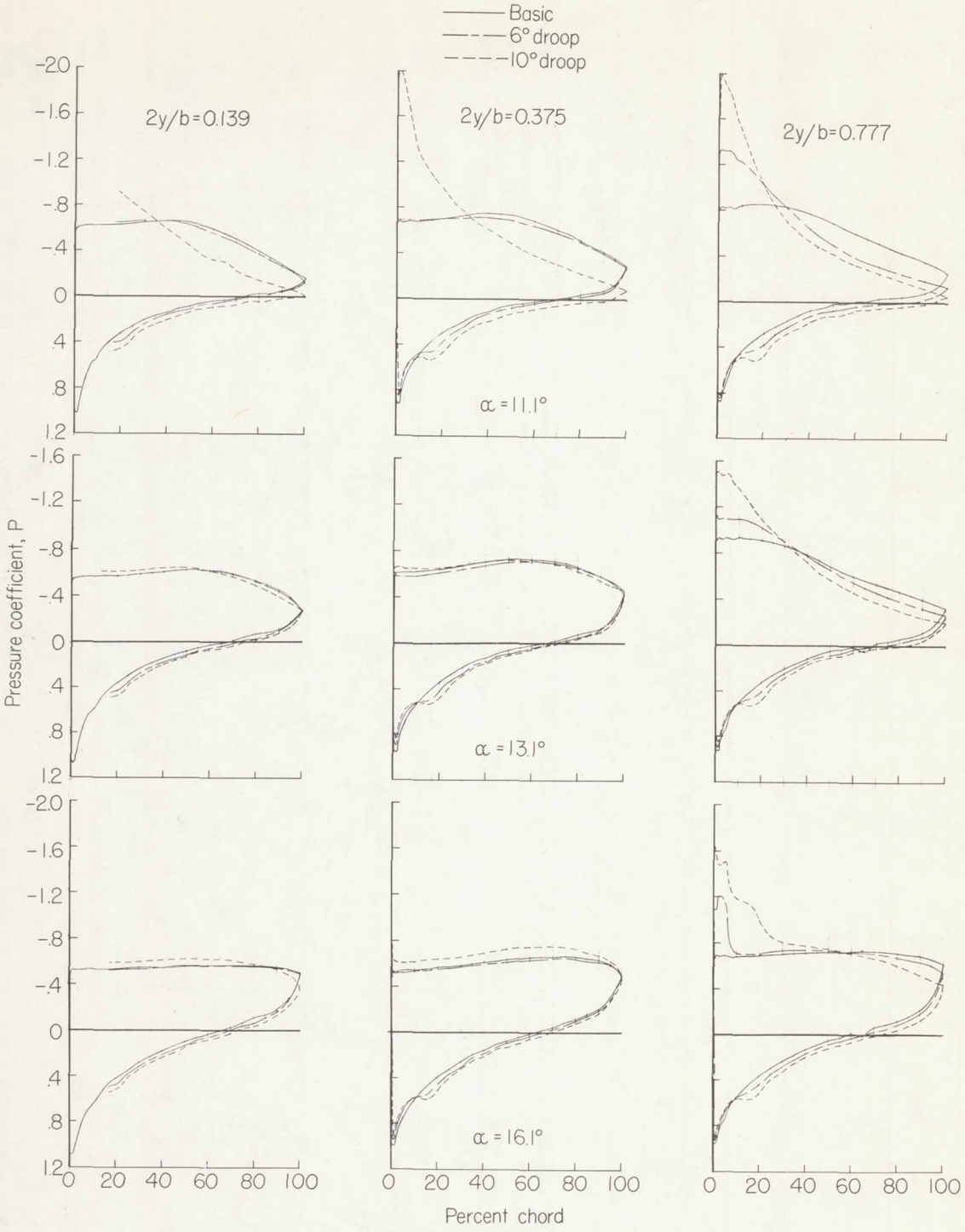


Figure 4.- Effect of leading-edge droop on base-pressure coefficient.



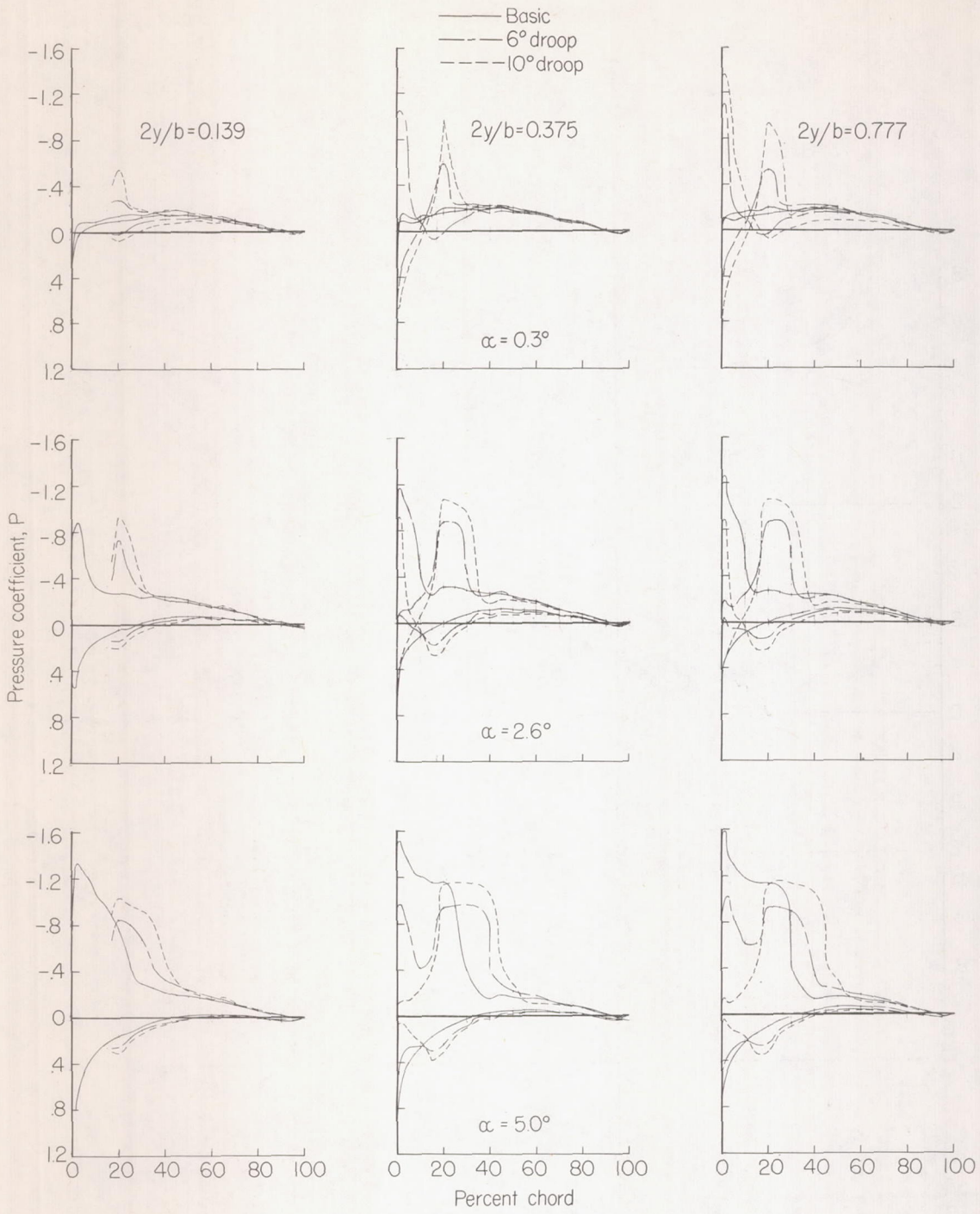
(a) M = 0.60; P_{cr} = -1.29.

Figure 5.- Effect of leading-edge droop on the pressure-coefficient distribution for the wing.



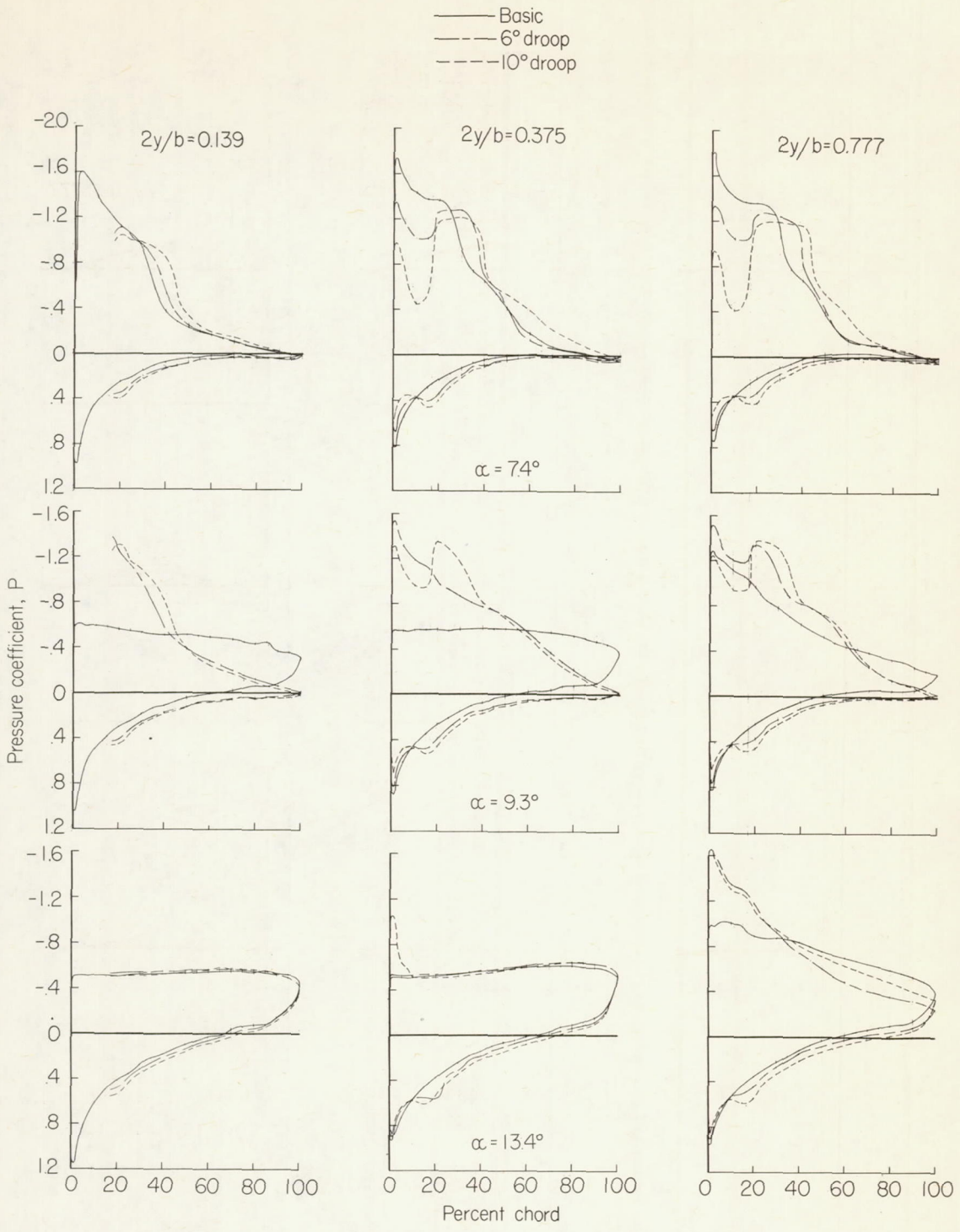
(a) Concluded.

Figure 5.- Continued.



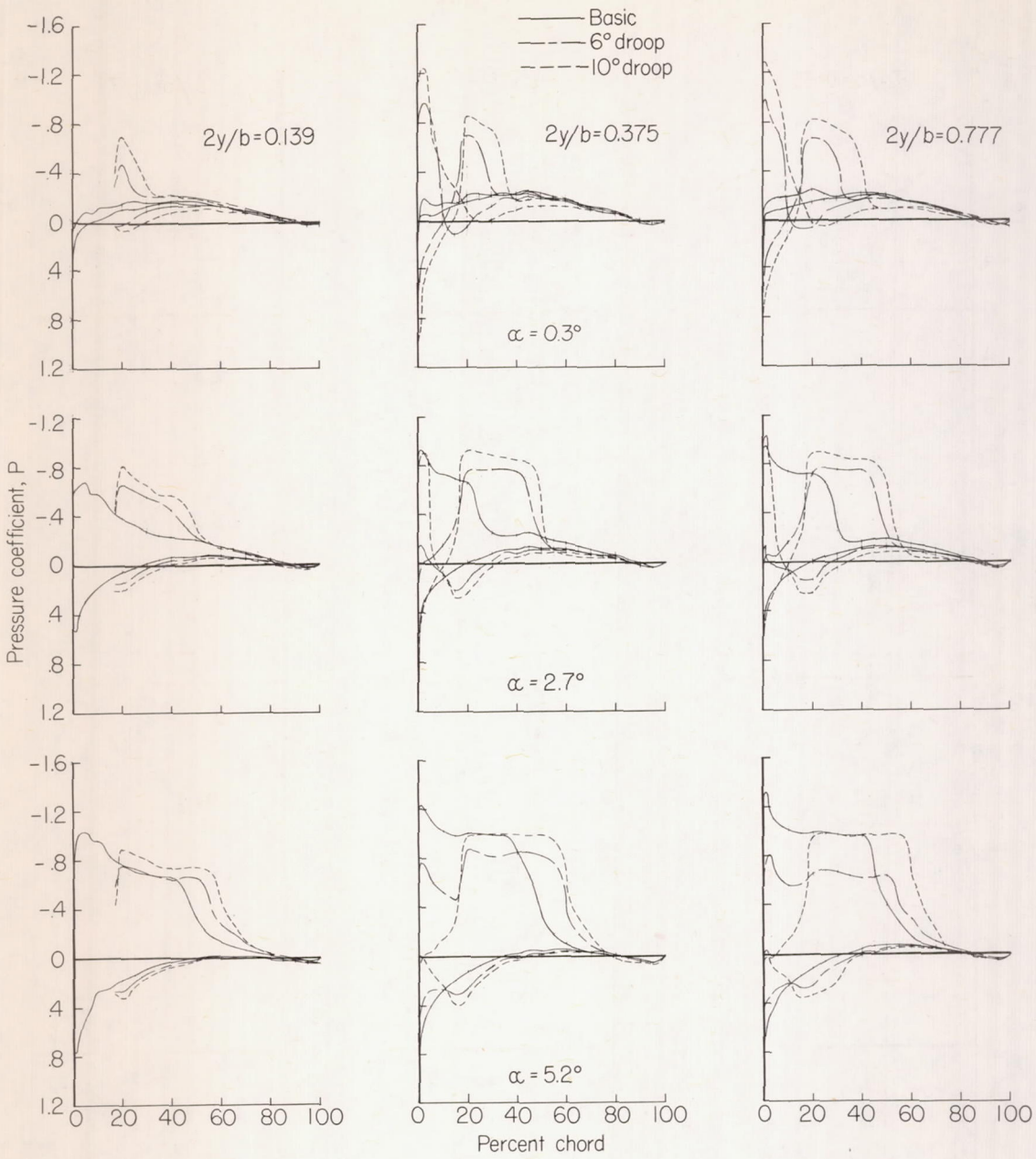
(b) M = 0.80; P_{cr} = -0.44.

Figure 5.- Continued.



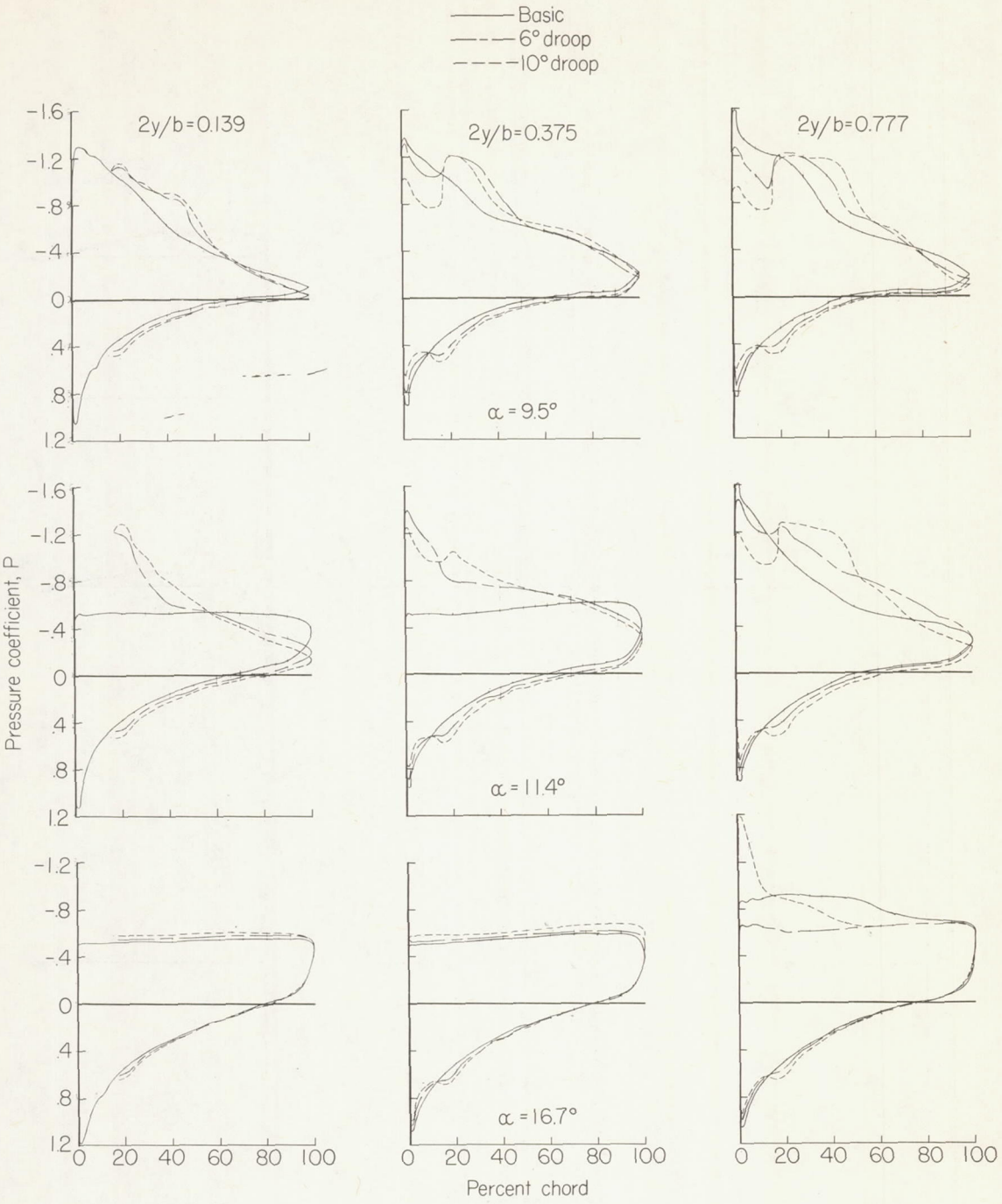
(b) Concluded.

Figure 5.- Continued.



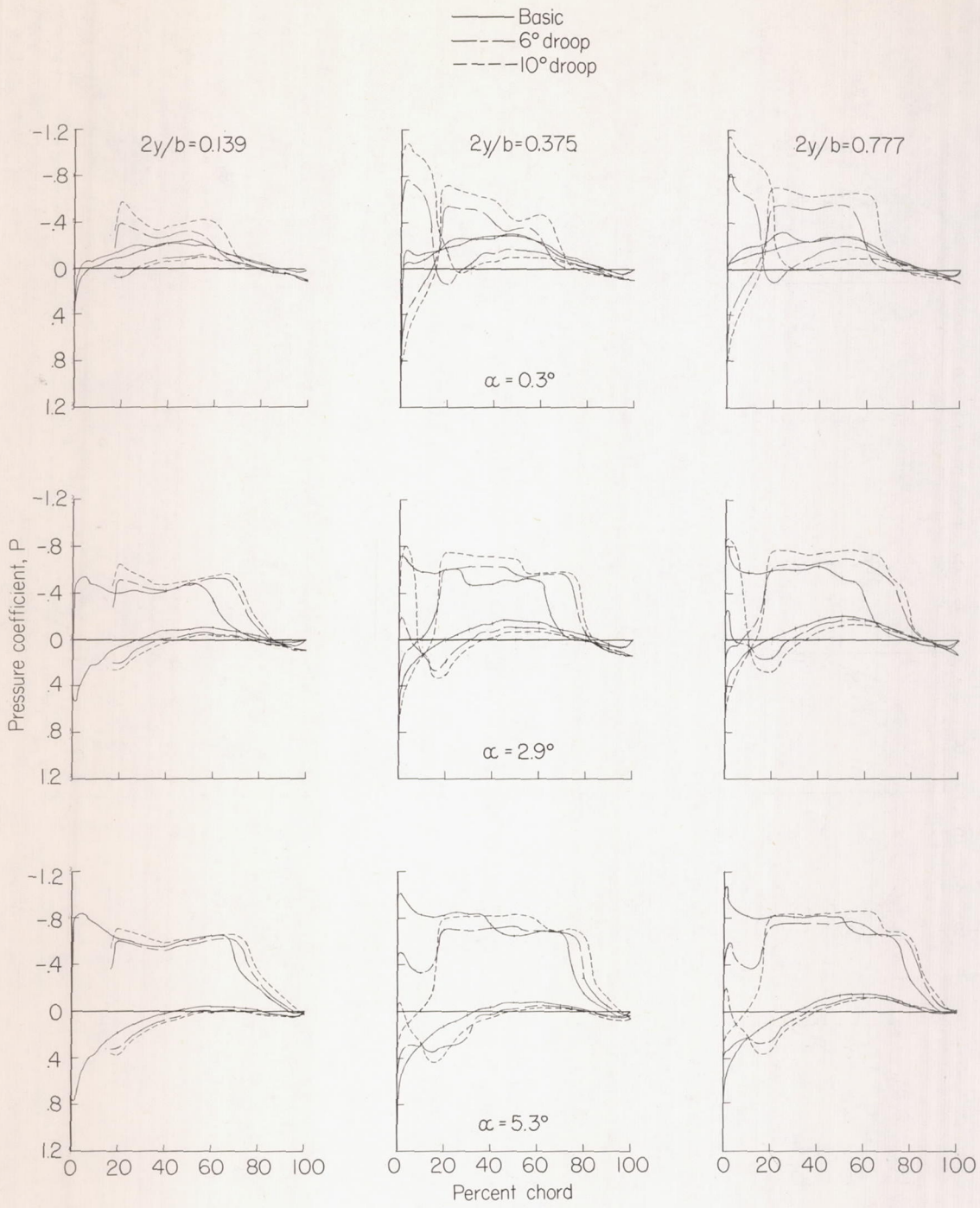
(c) M = 0.85; P_{cr} = -0.30.

Figure 5.- Continued.



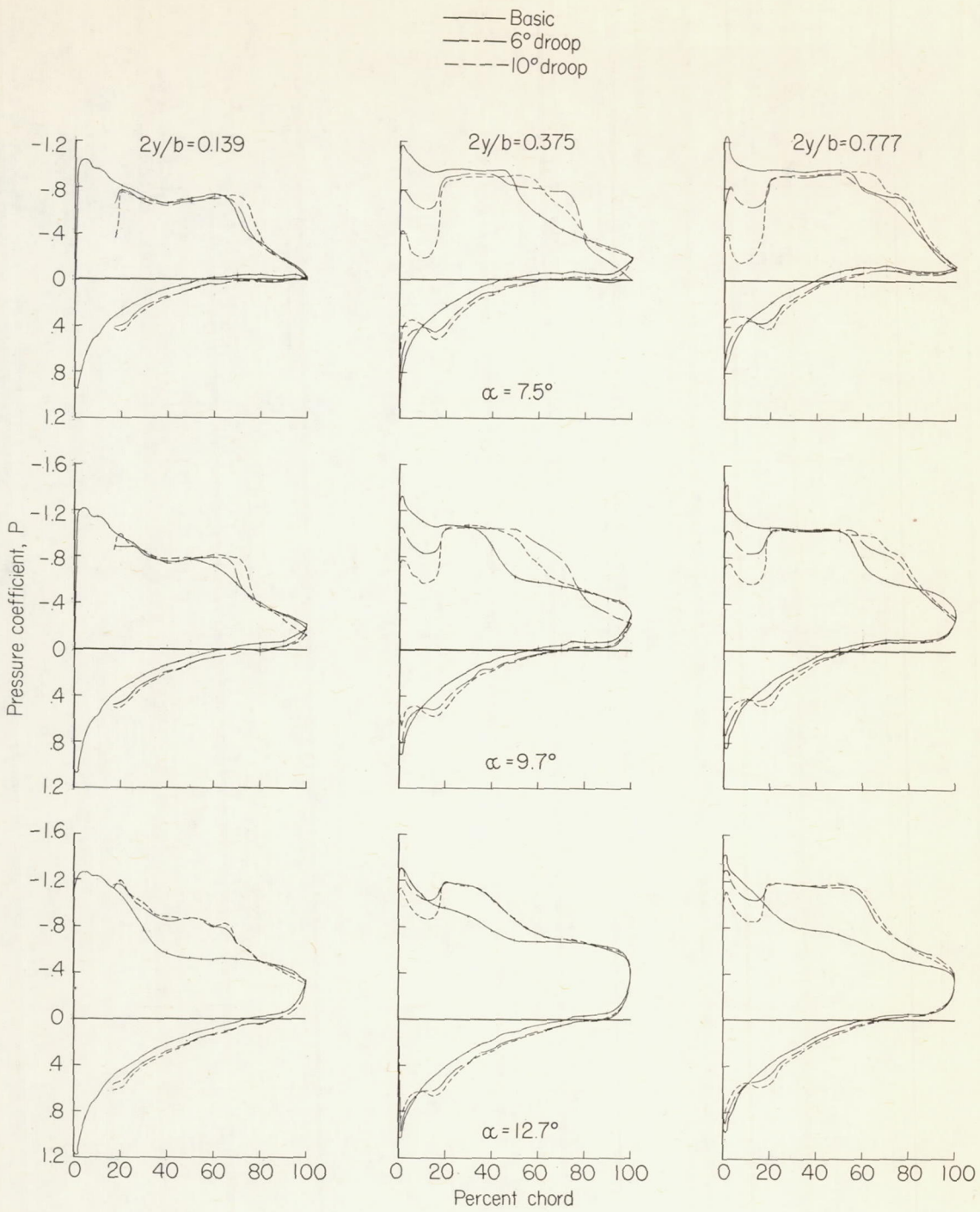
(c) Concluded.

Figure 5.- Continued.



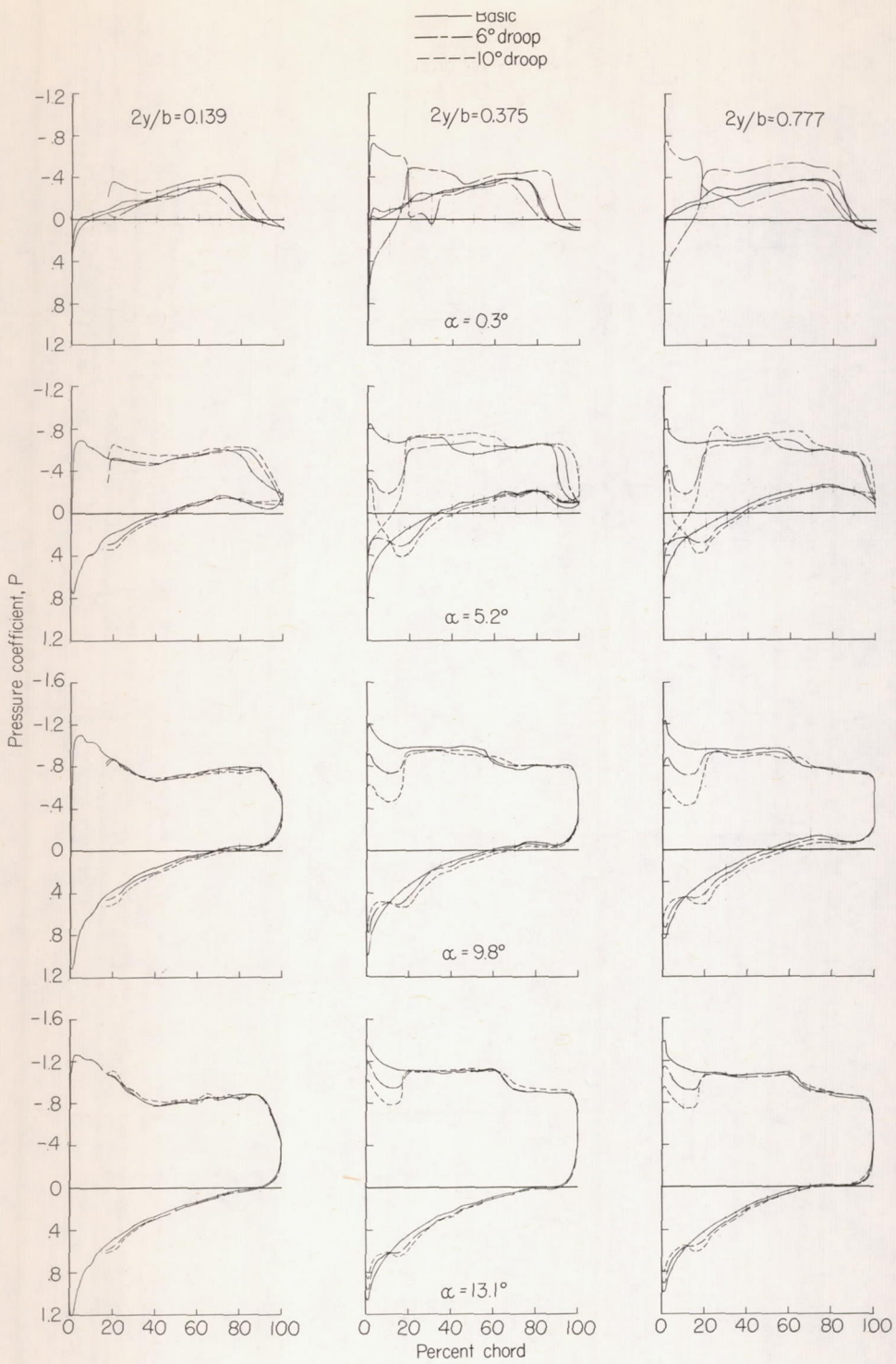
(d) M = 0.90; P_{cr} = -0.18.

Figure 5.- Continued.



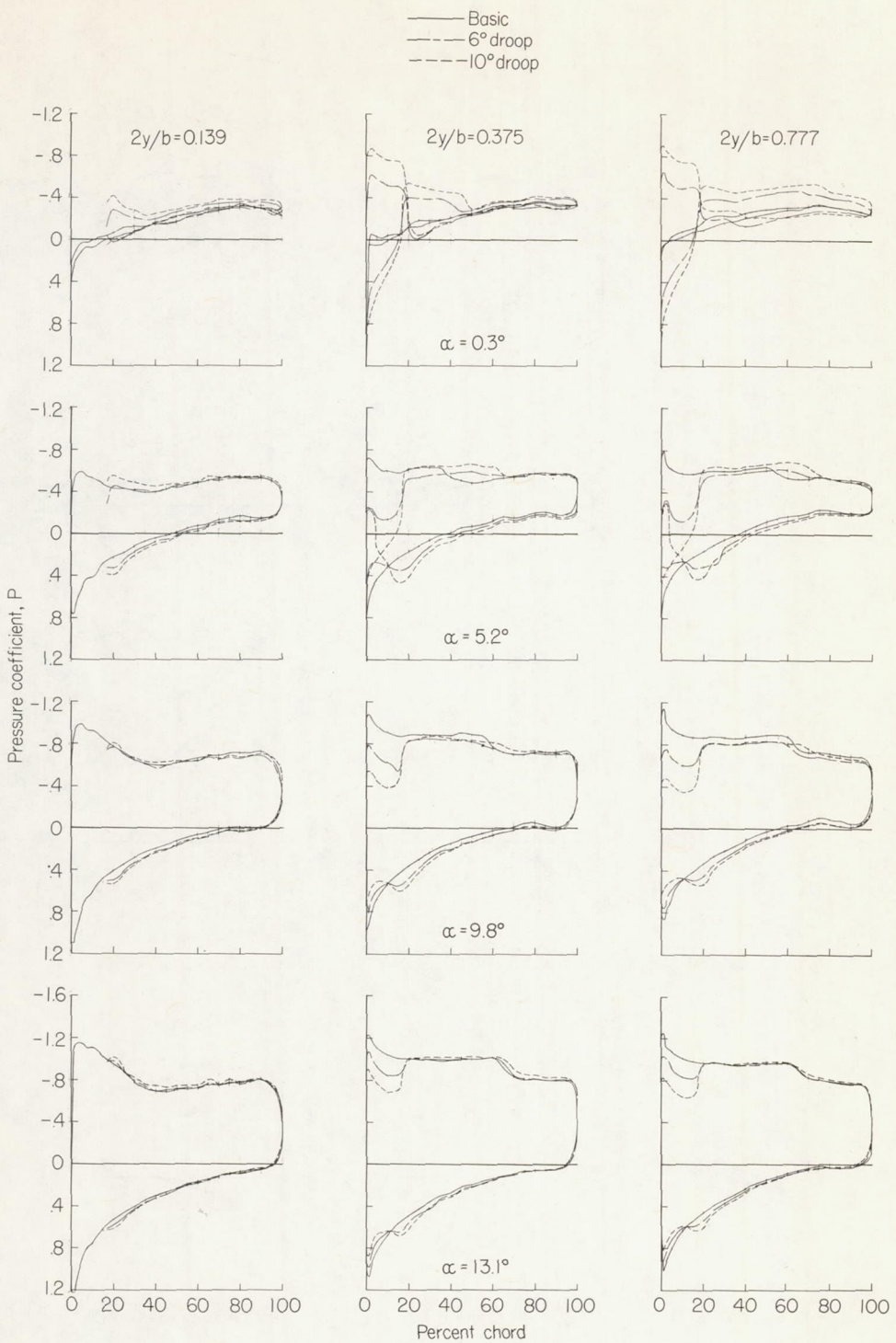
(d) Concluded.

Figure 5.- Continued.



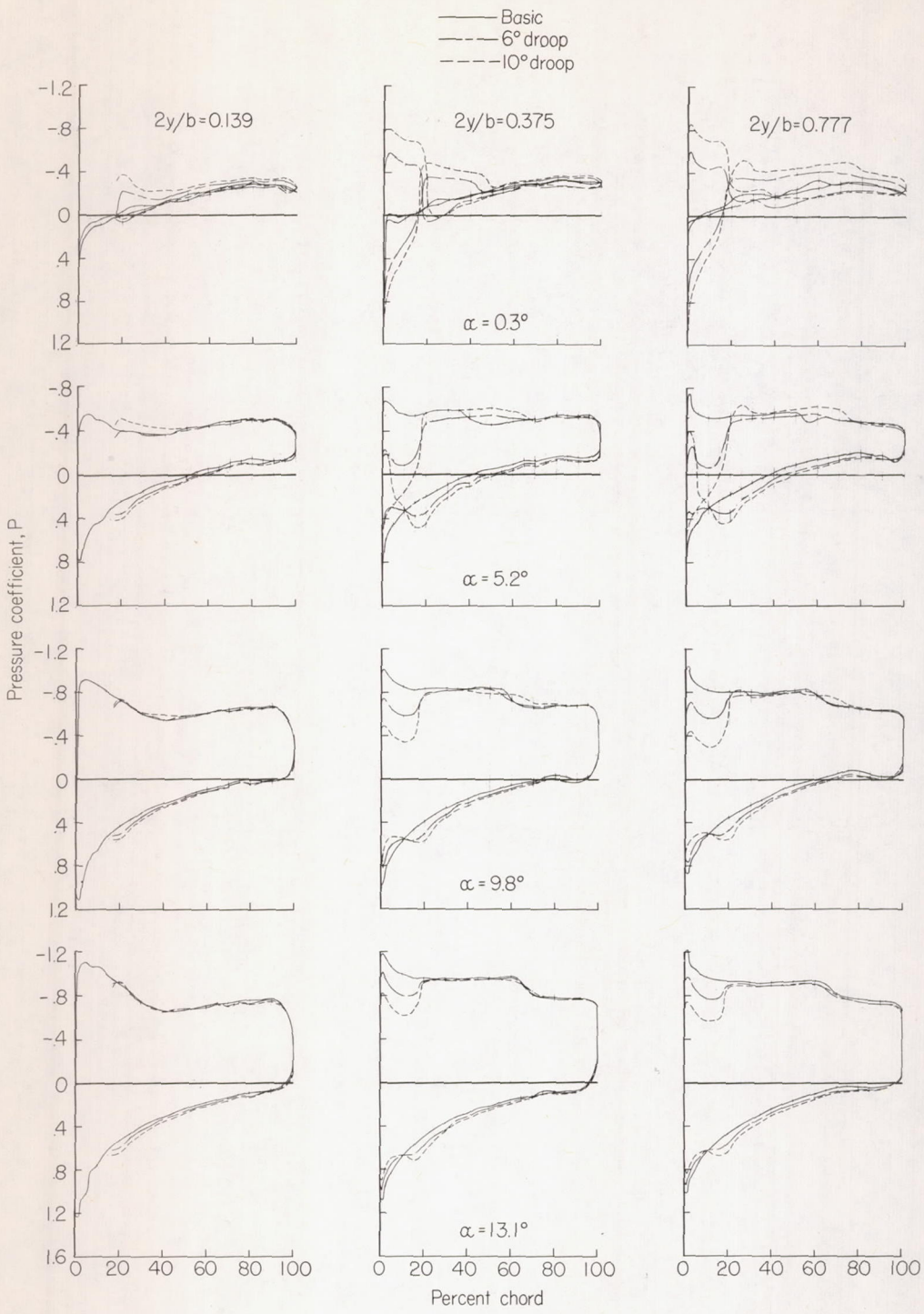
(e) $M = 0.94$; $P_{cr} = -0.10$.

Figure 5.- Continued.



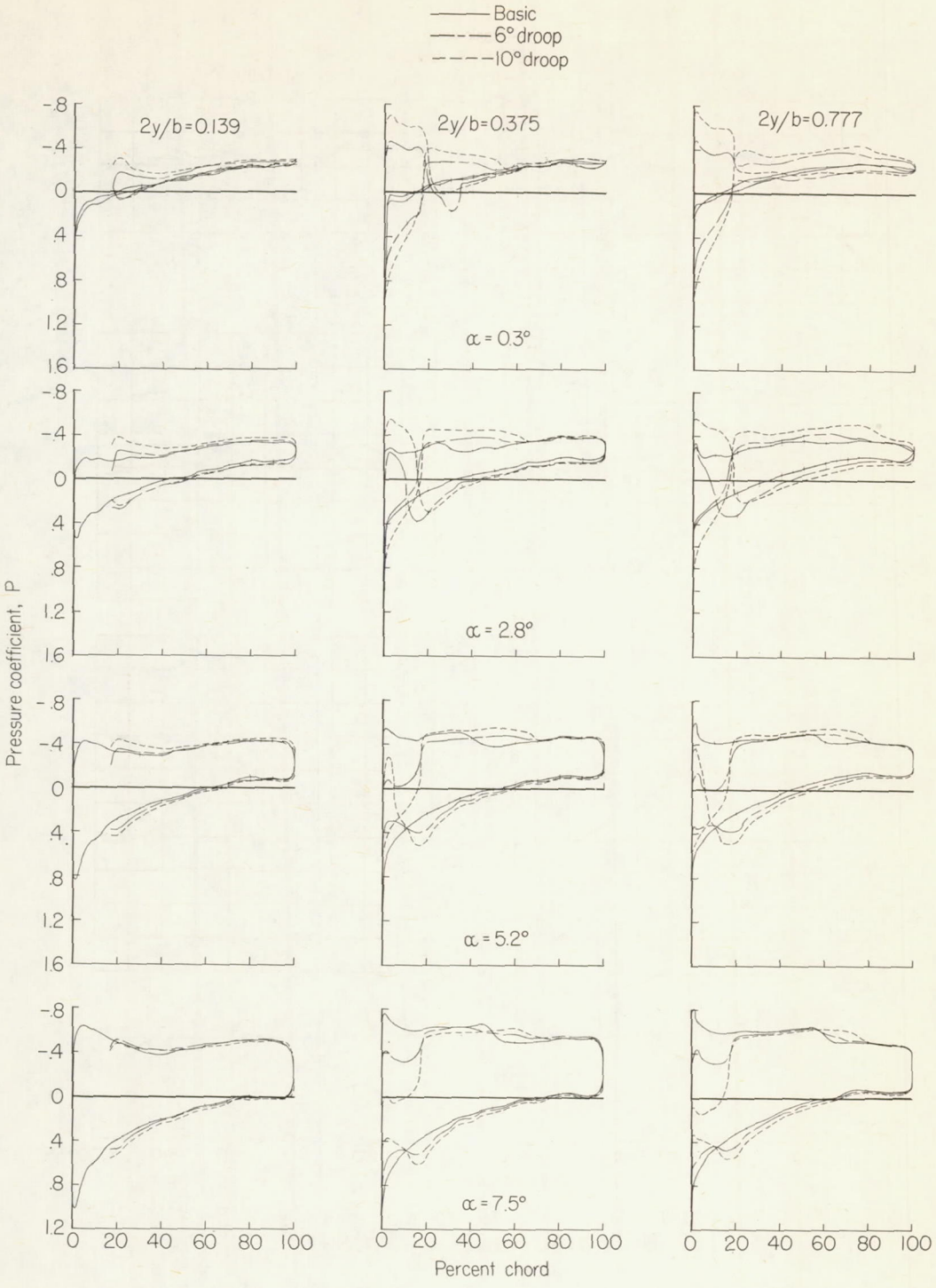
(f) M = 0.98; P_{cr} = -0.03.

Figure 5.- Continued.



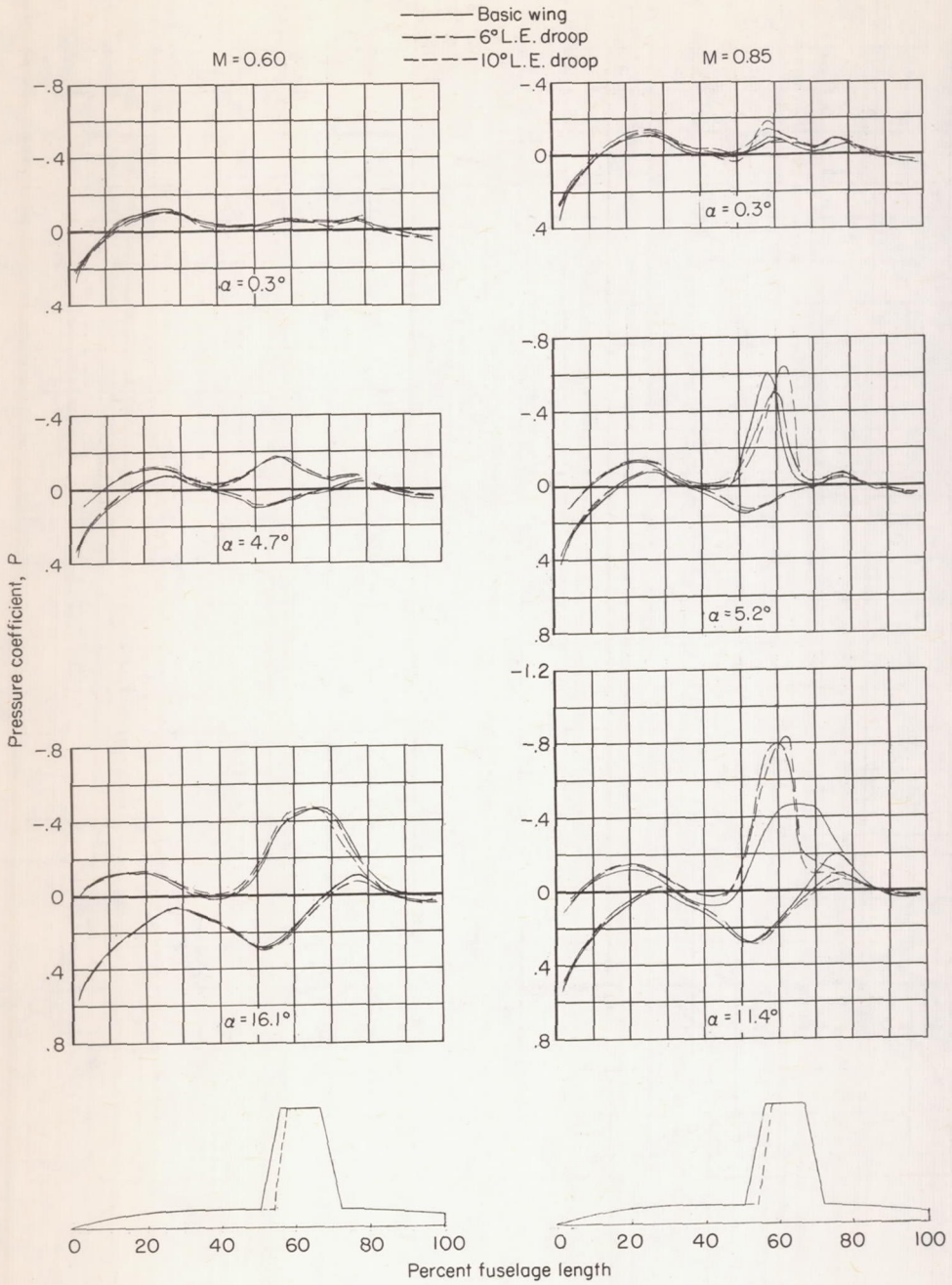
(g) M = 1.00; P_{cr} = 0.

Figure 5.- Continued.



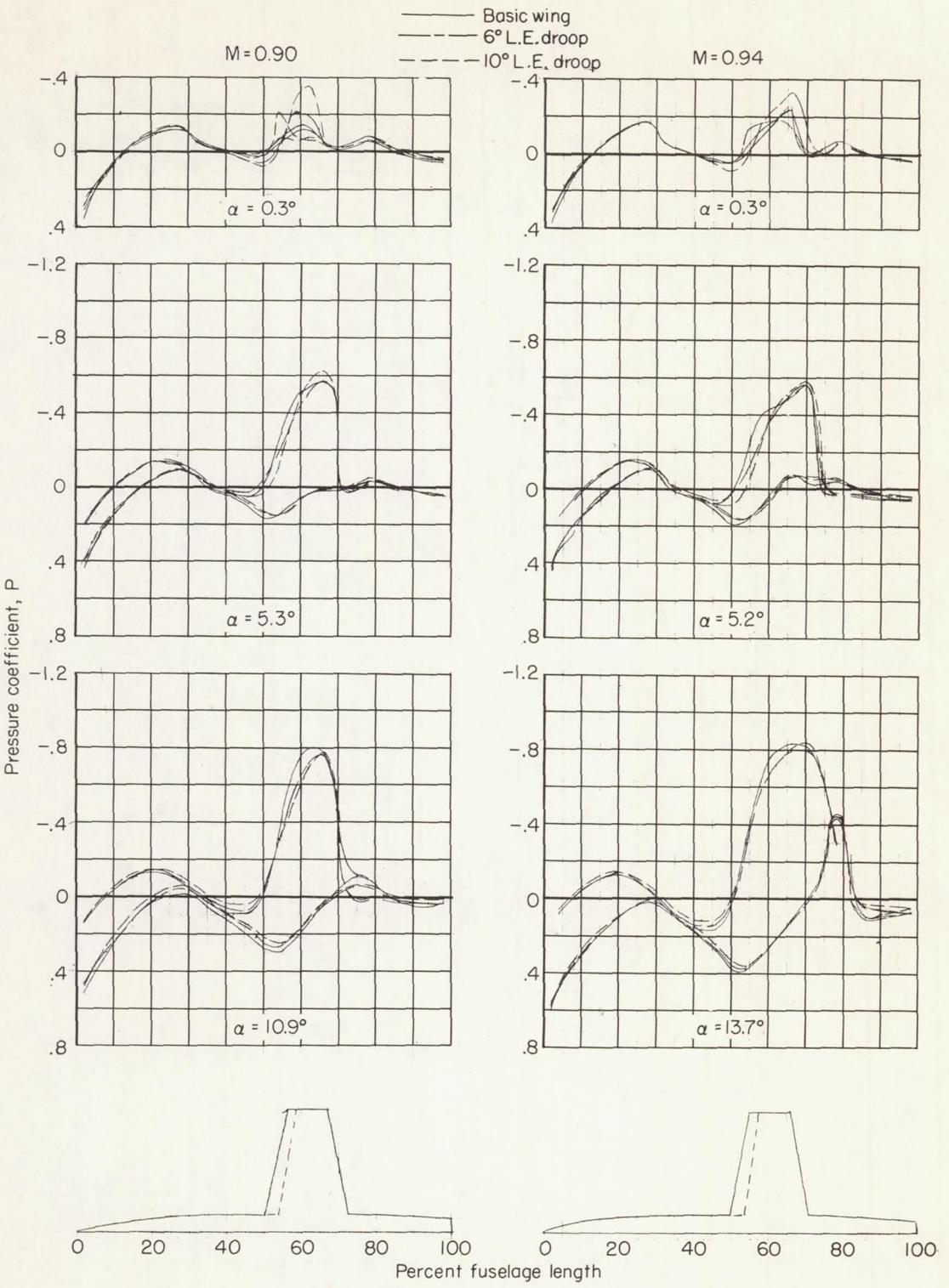
(h) M = 1.05.

Figure 5.- Concluded.



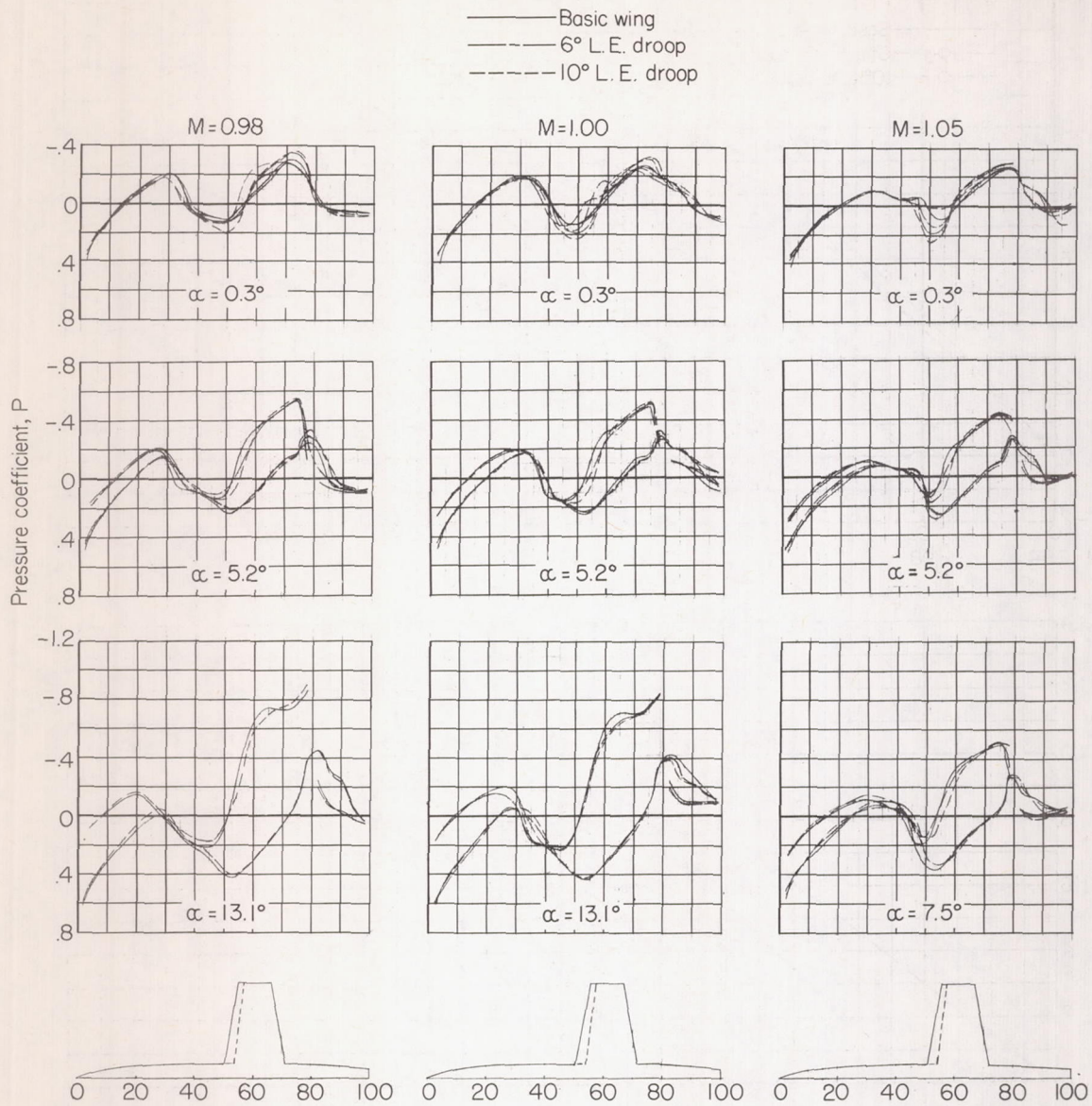
(a) M = 0.60 and M = 0.85.

Figure 6.- Effect of leading-edge droop on the pressure-coefficient distributions for the fuselage.



(b) M = 0.90 and M = 0.94.

Figure 6.- Continued.



(c) M = 0.98, M = 1.00, and M = 1.05.

Figure 6.- Concluded.

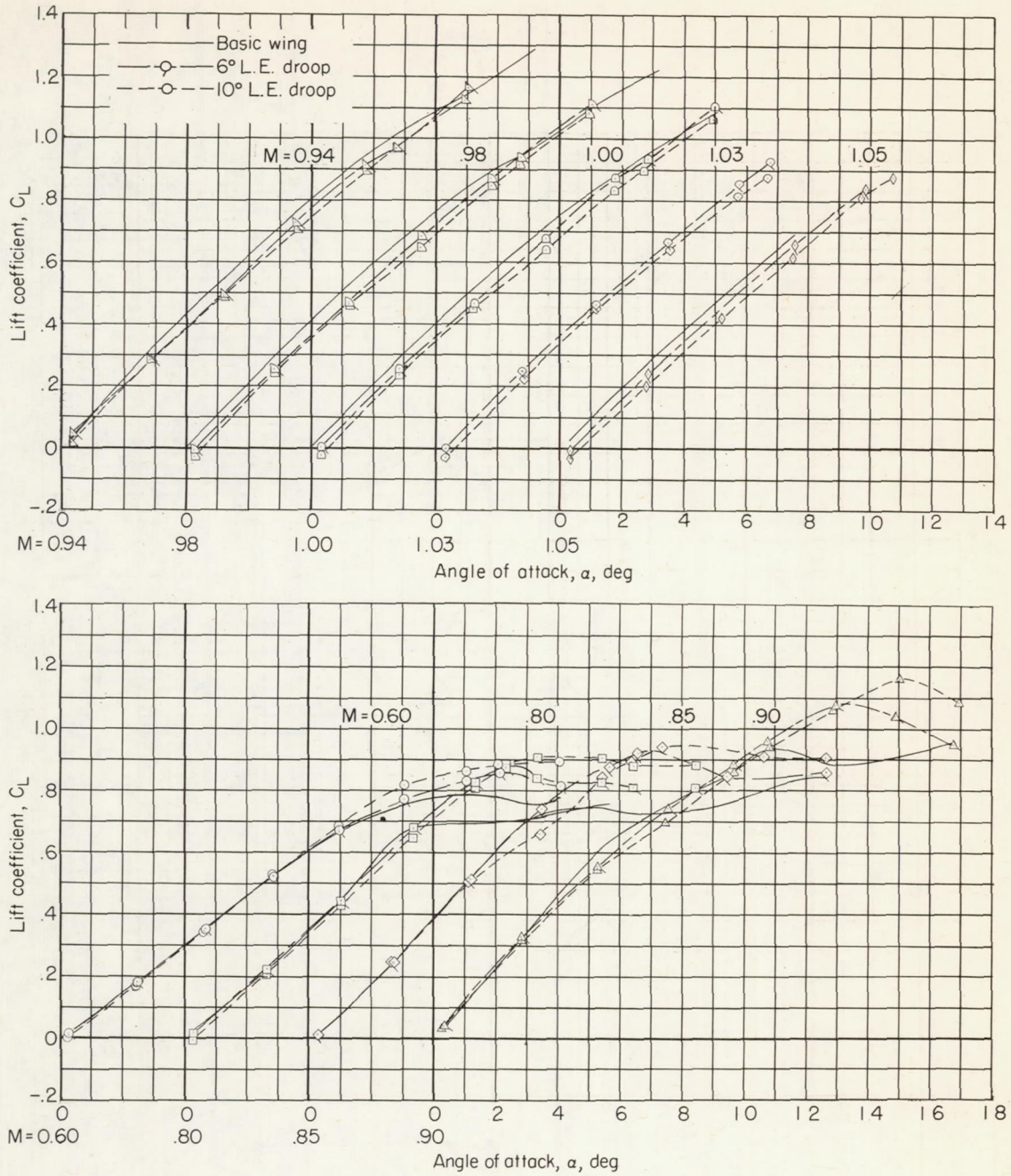


Figure 7.- Effect of leading-edge droop on the lift characteristics.

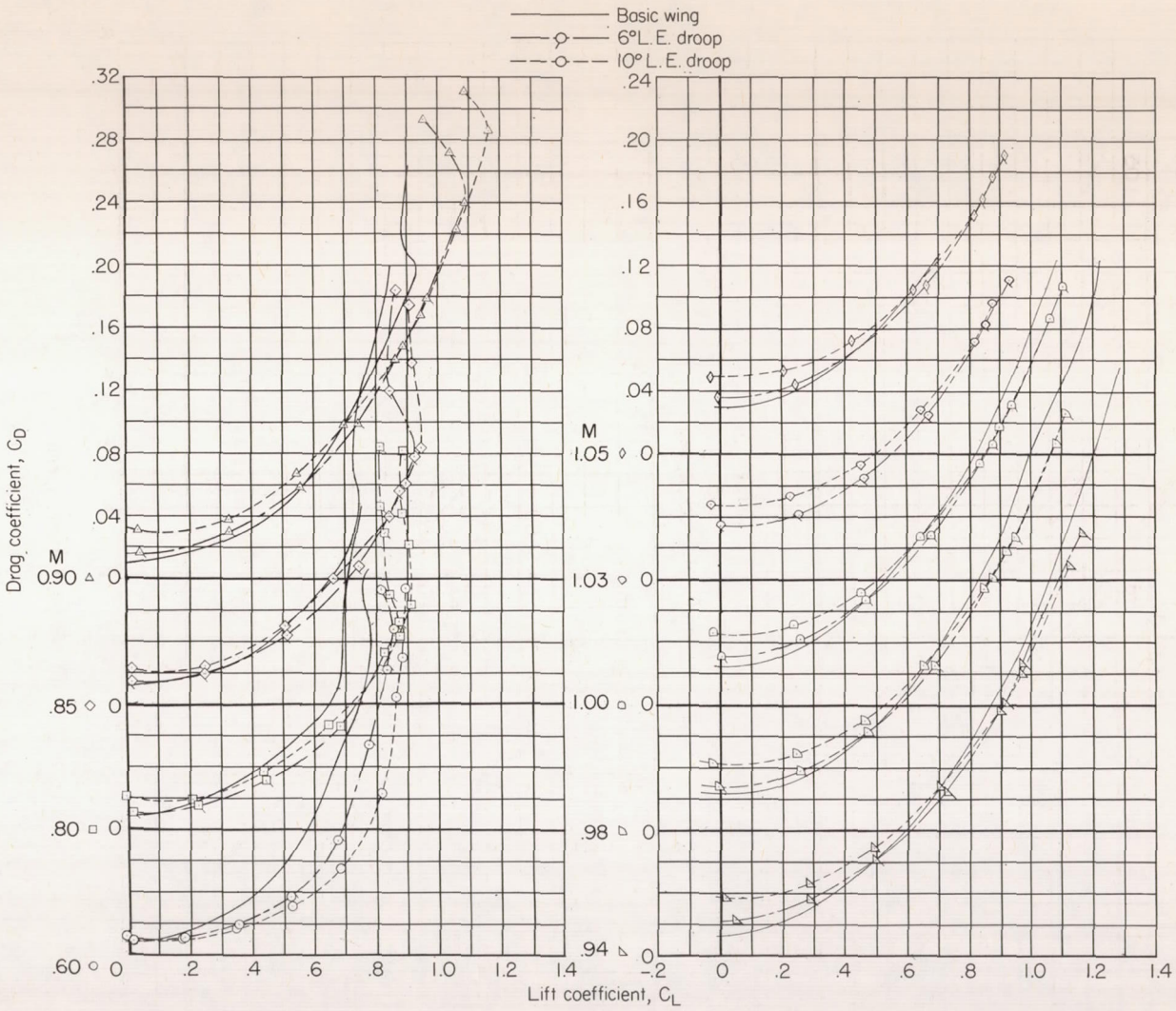


Figure 8.- Effect of leading-edge droop on the drag characteristics.

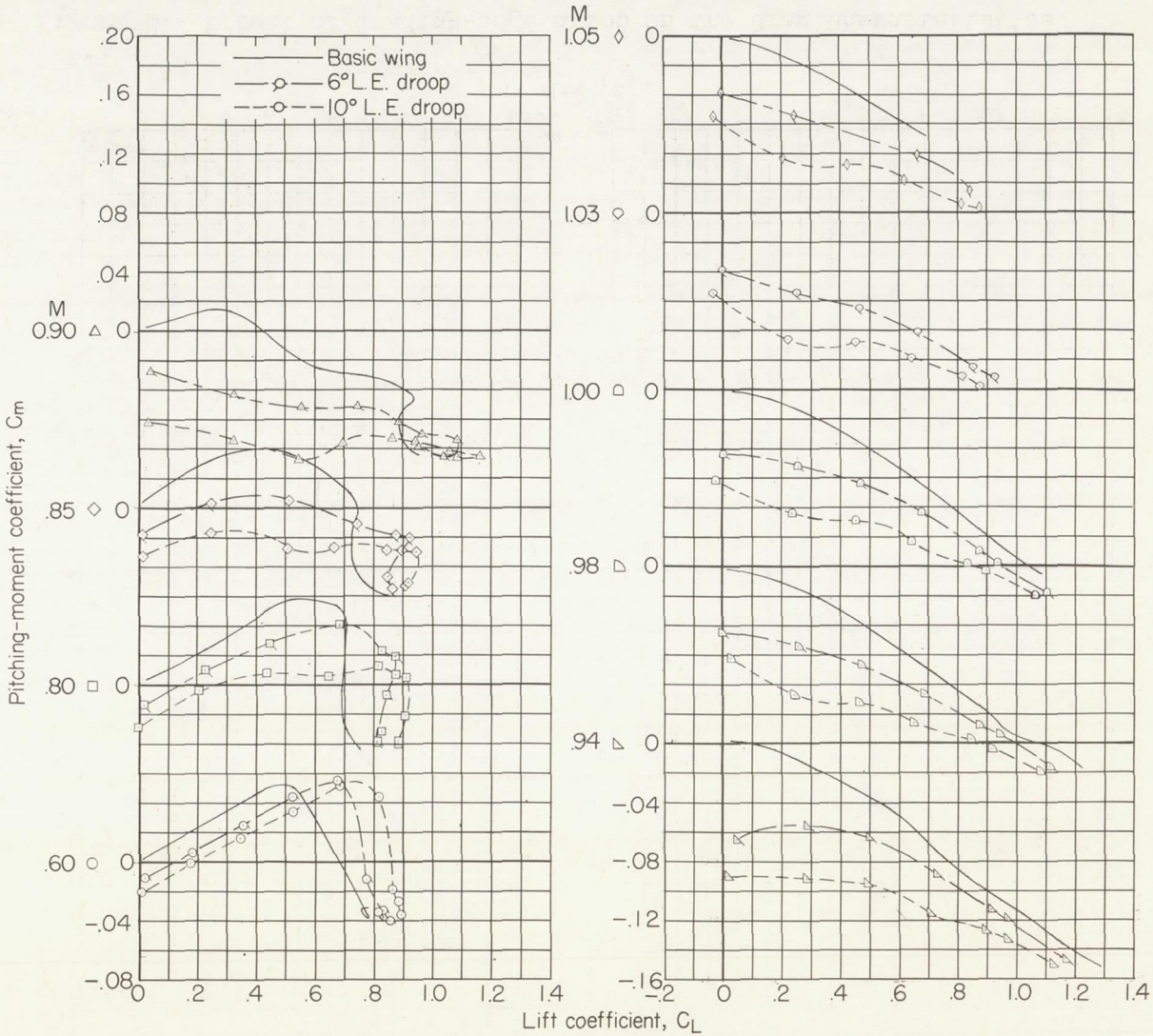


Figure 9.- Effect of leading-edge droop on pitching-moment characteristics.

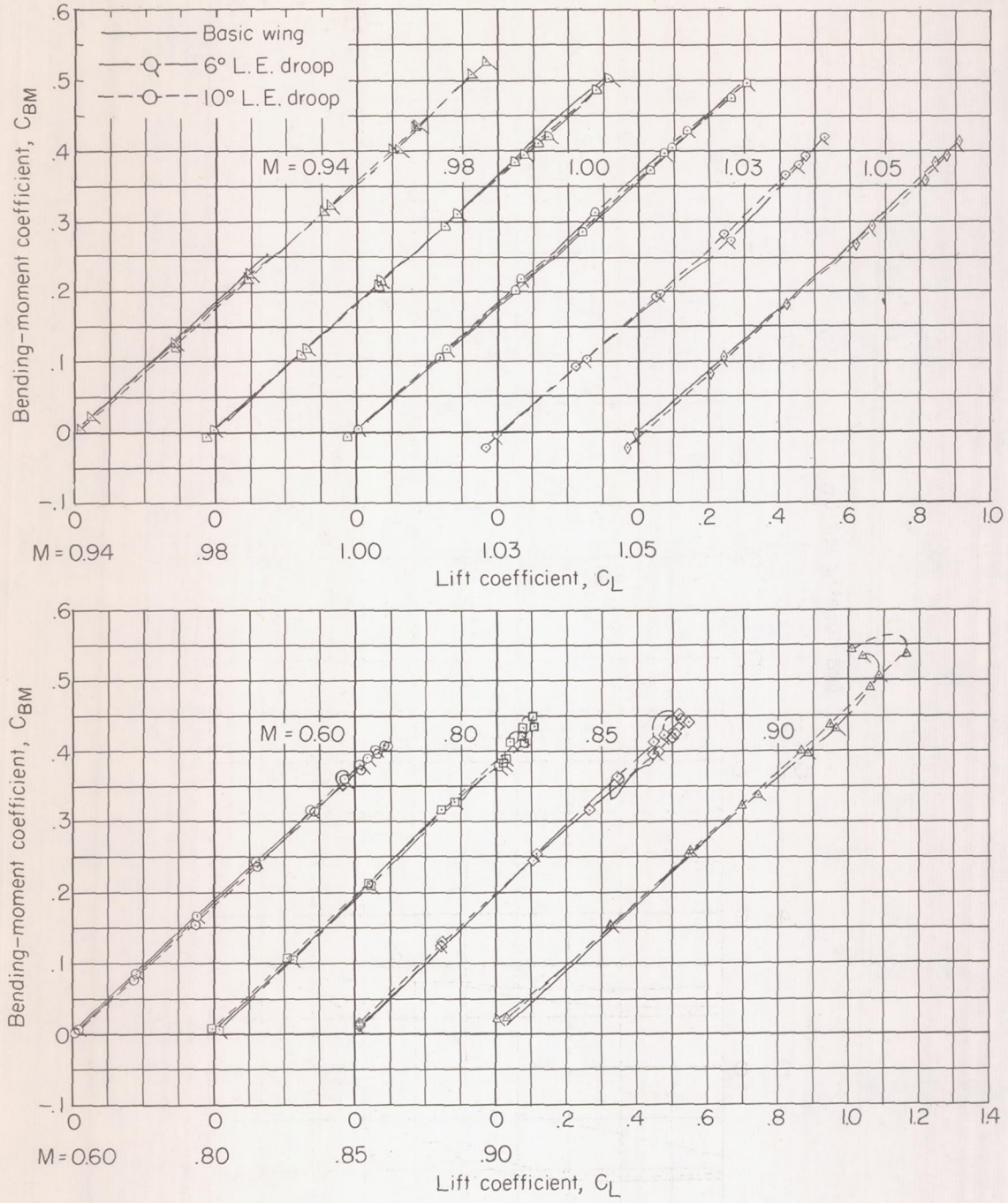


Figure 10.- Effect of leading-edge droop on wing-panel bending-moment coefficient.

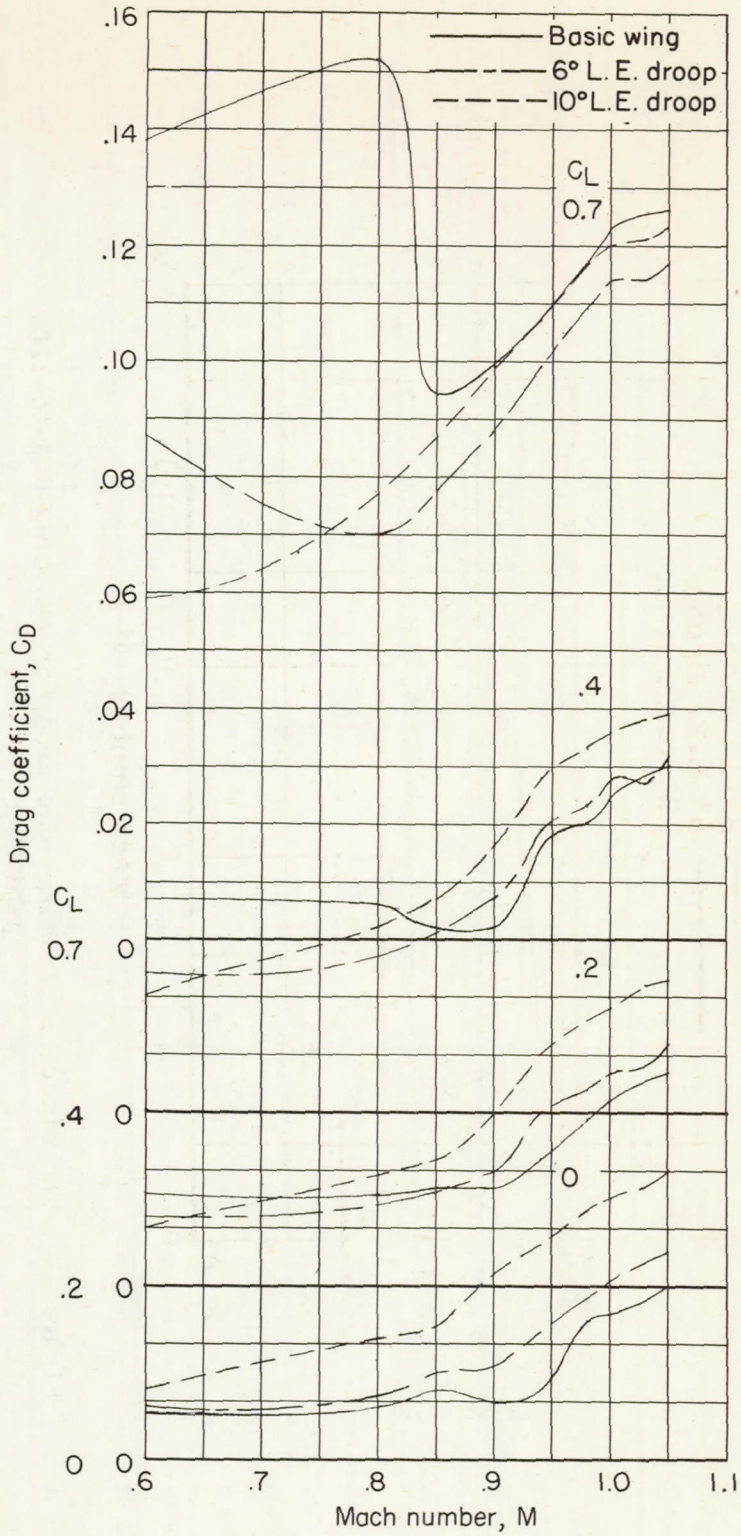


Figure 11.- Effect of leading-edge droop on drag coefficient at several lift coefficients.

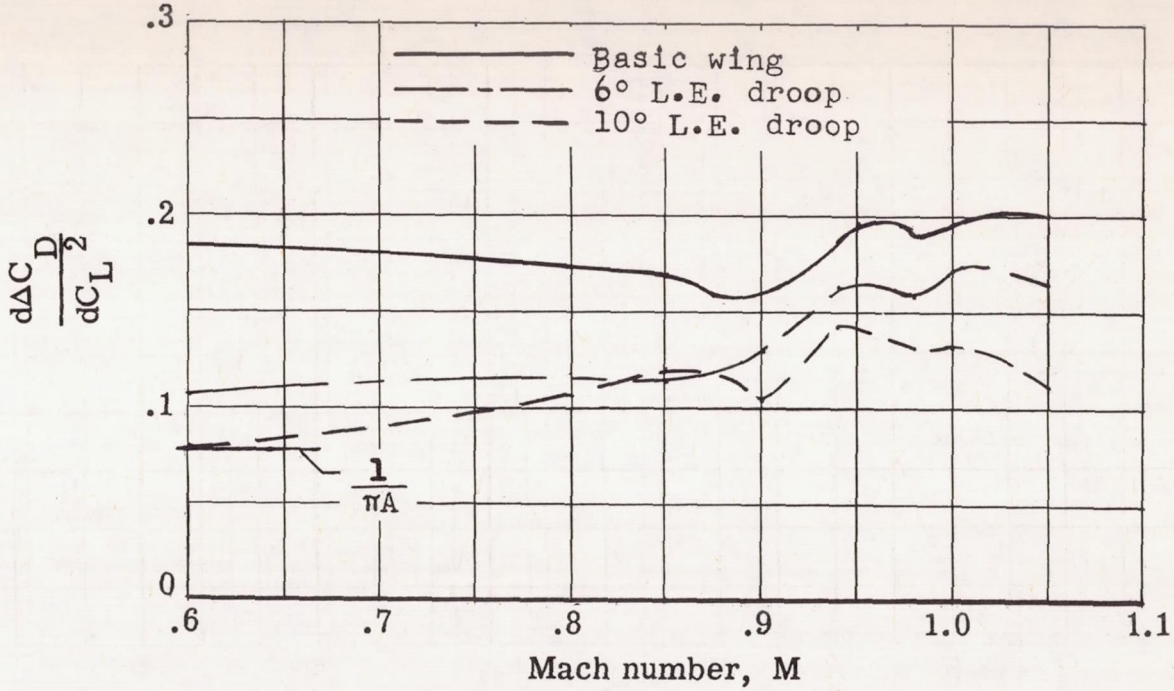


Figure 12.- The effect of leading-edge droop on the drag-due-to-lift parameter.

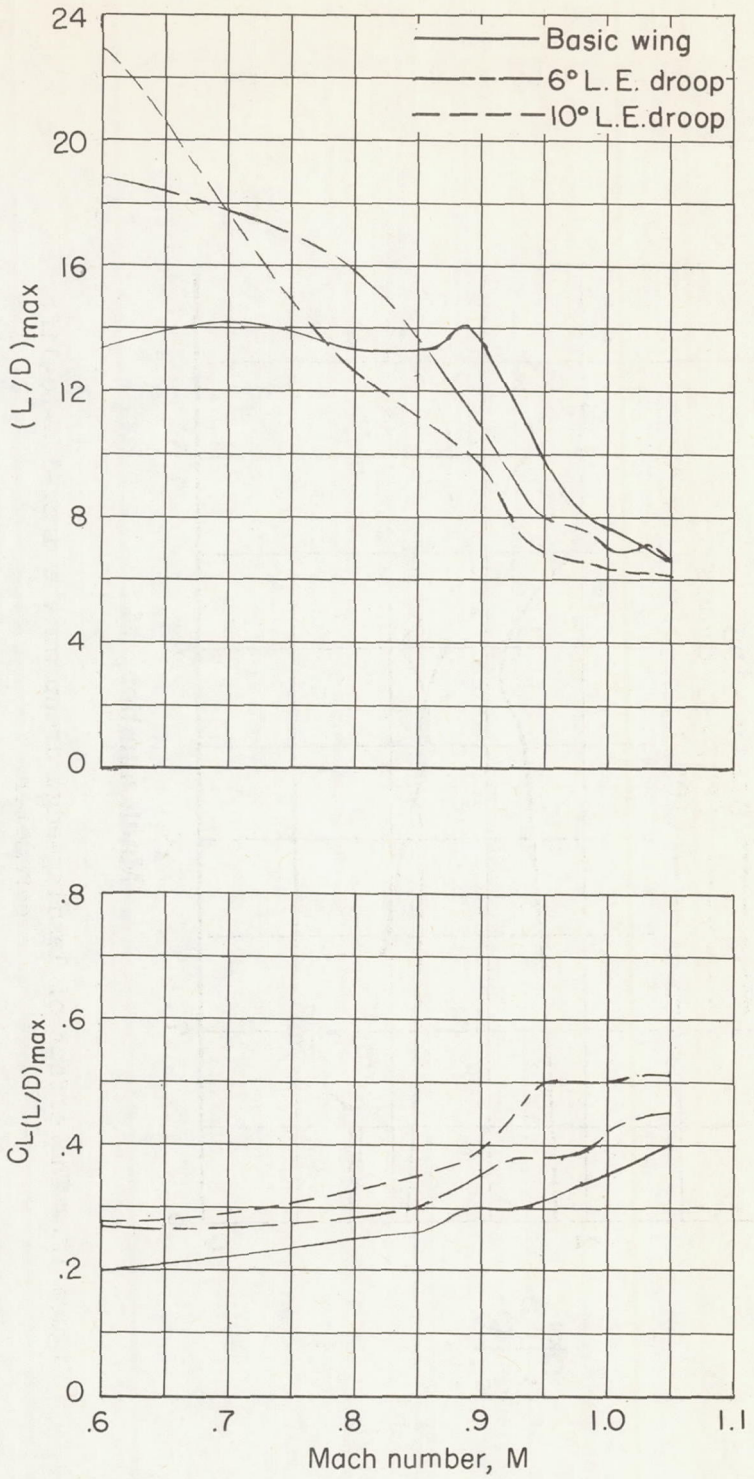


Figure 13.- Effect of leading-edge droop on $(L/D)_{max}$ and lift coefficient for $(L/D)_{max}$.

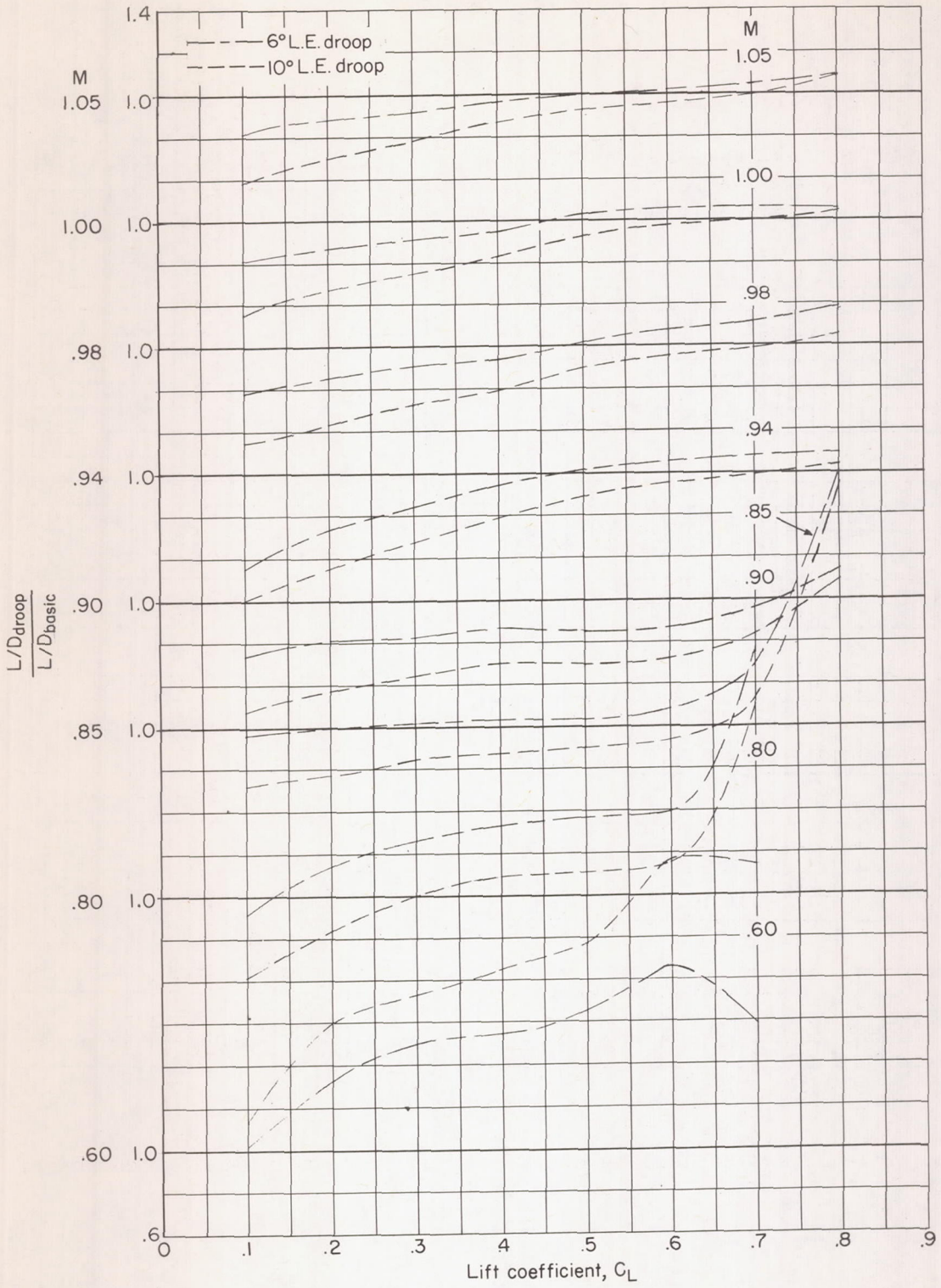


Figure 14.- Variation with lift coefficient of the ratio of L/D for models with leading-edge droop to L/D for the model with basic wing.

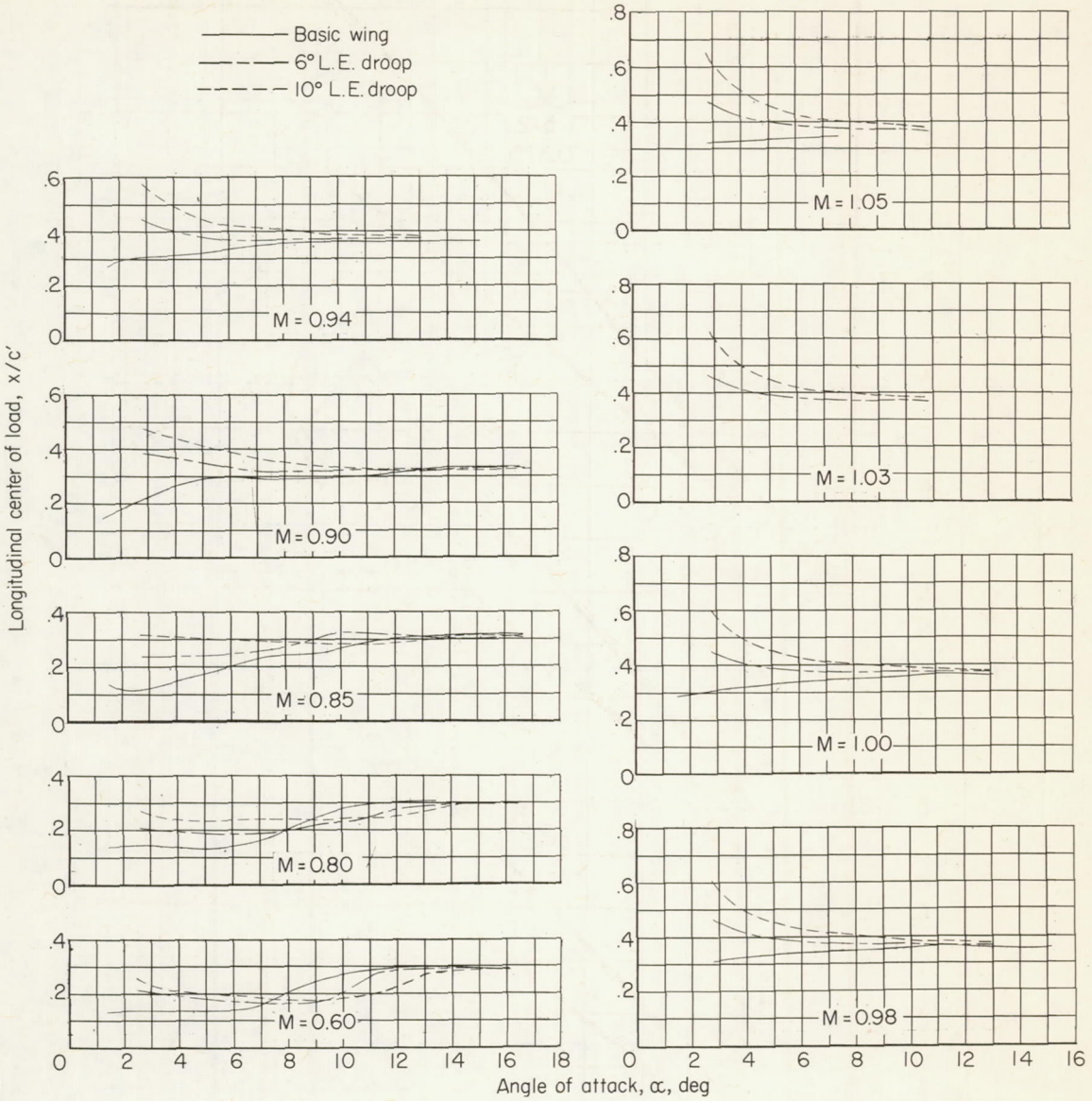


Figure 15.- Effect of leading-edge droop on the longitudinal location of center of load.

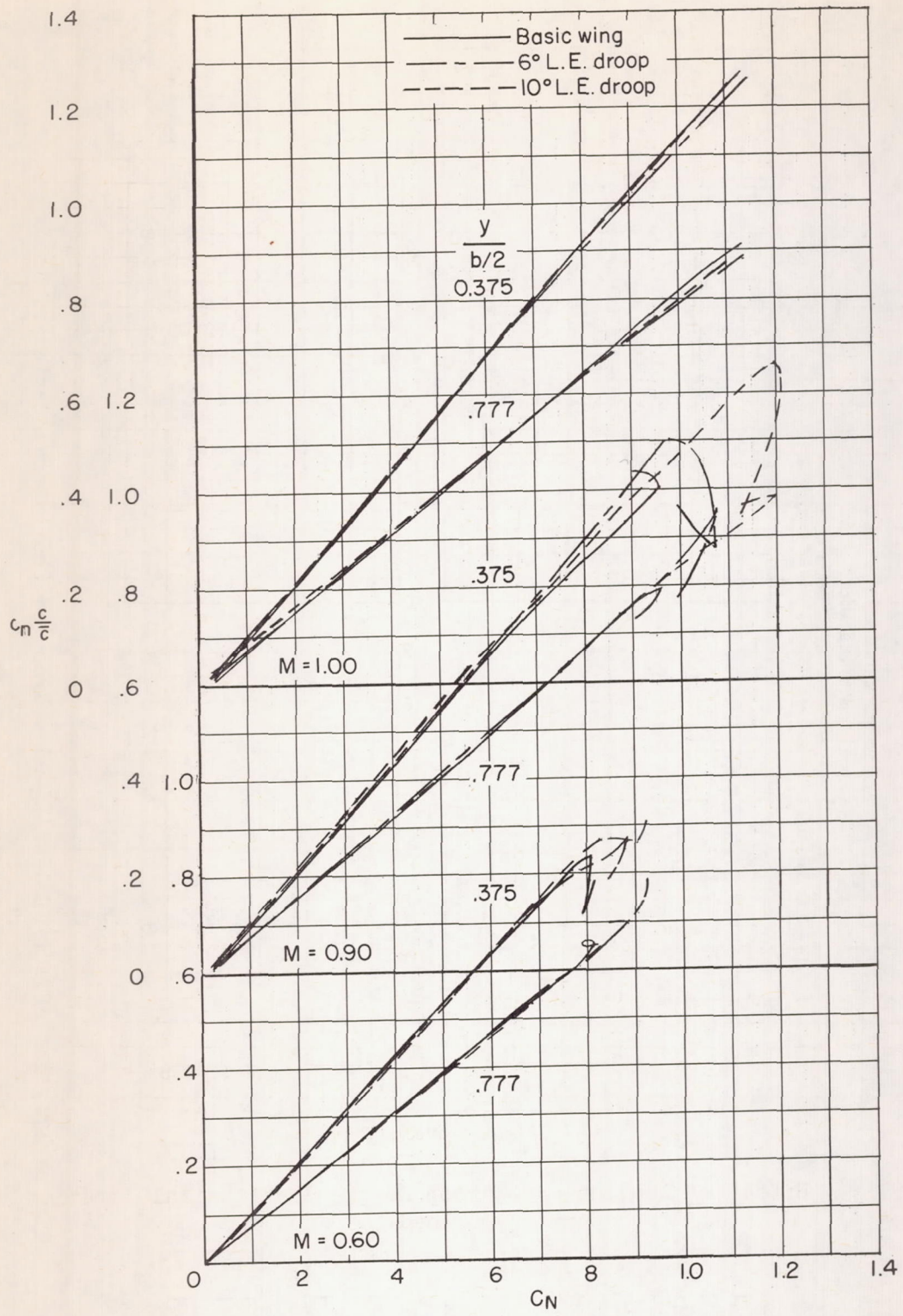


Figure 16.- The effect of leading-edge droop on the section normal-load parameter.

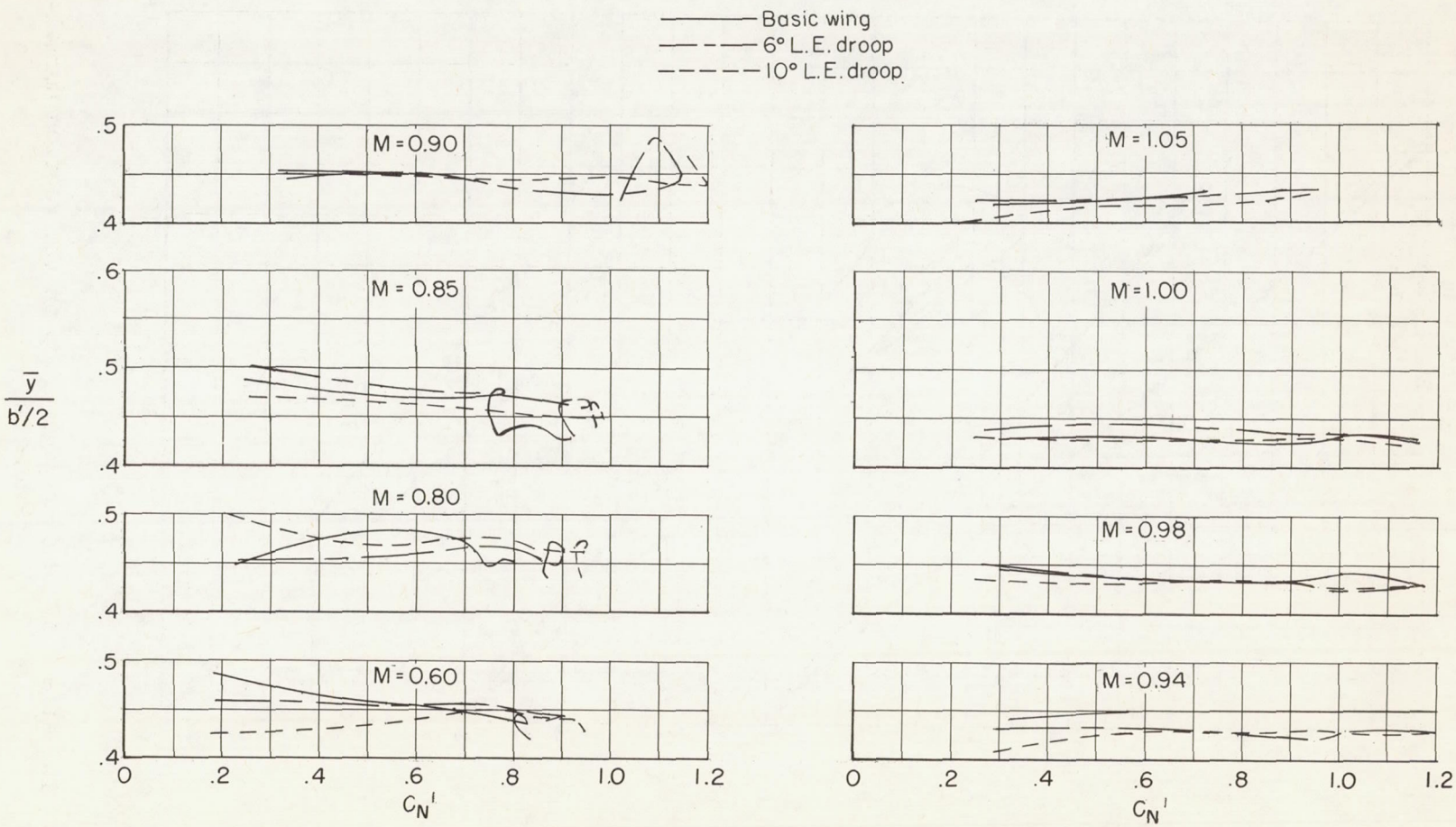
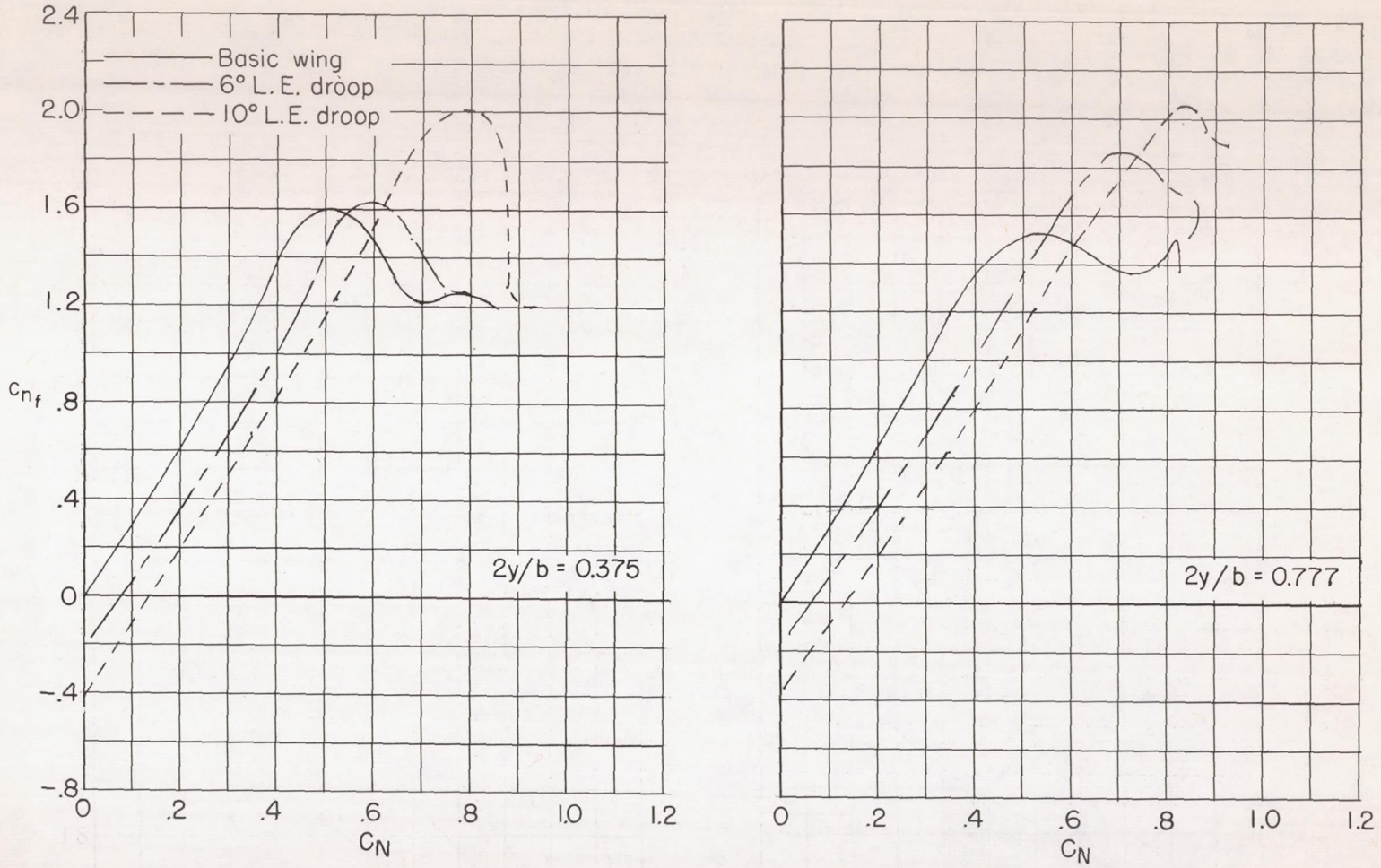
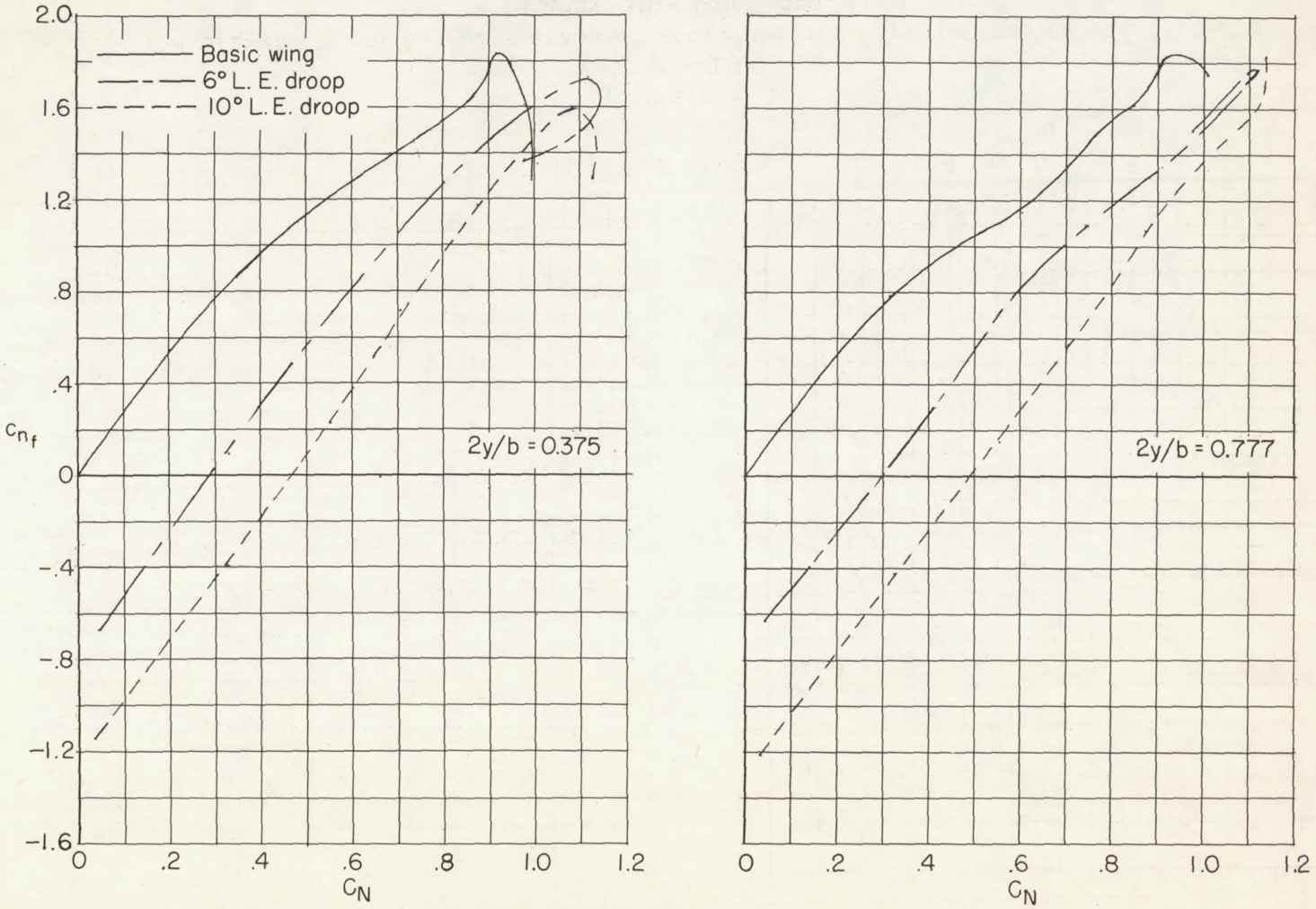


Figure 17.- The effect of leading-edge droop on the lateral center of load.



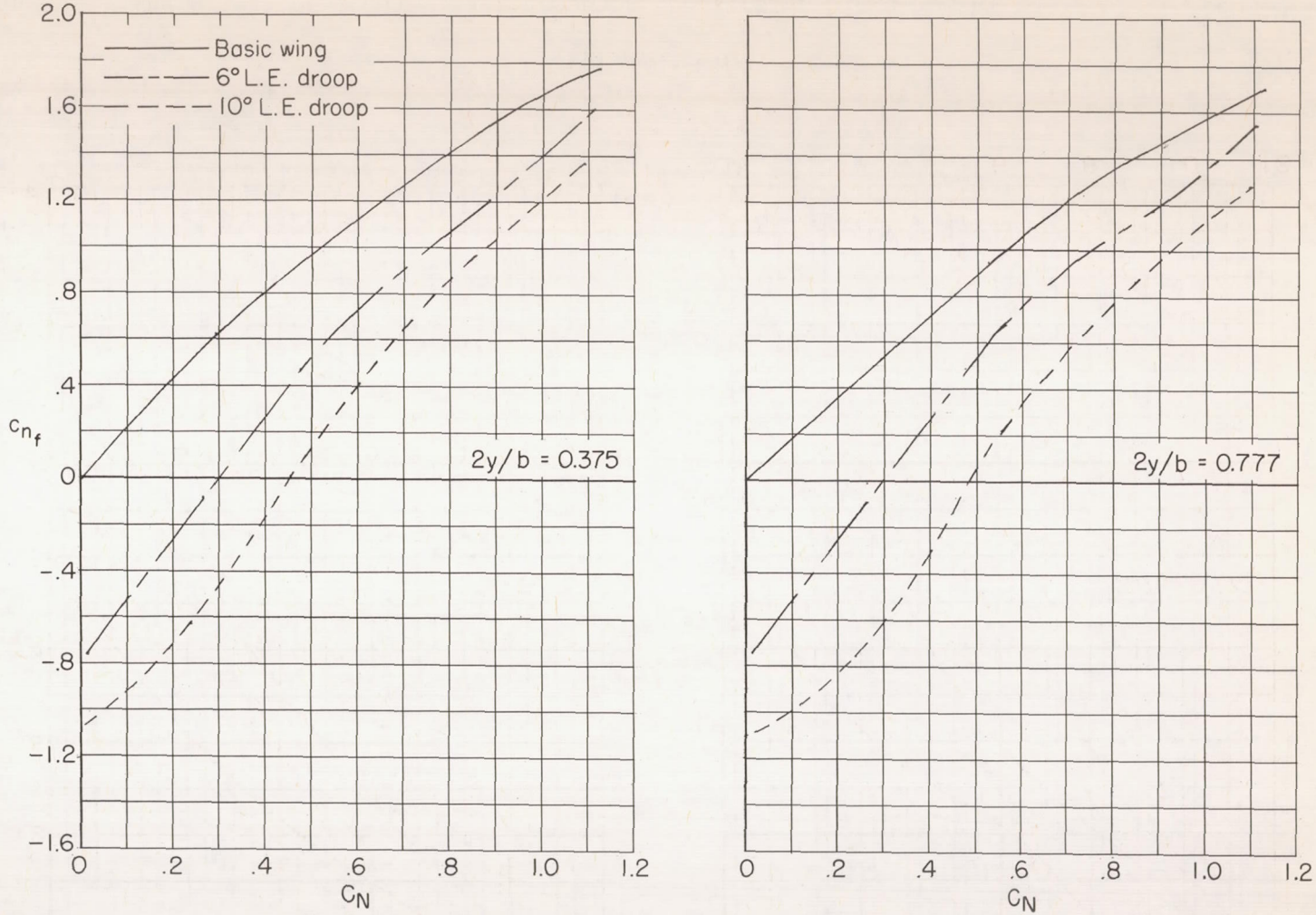
(a) M = 0.60.

Figure 18.- The effect of leading-edge droop on the section normal-force coefficient for the forward 17 percent of the wing.



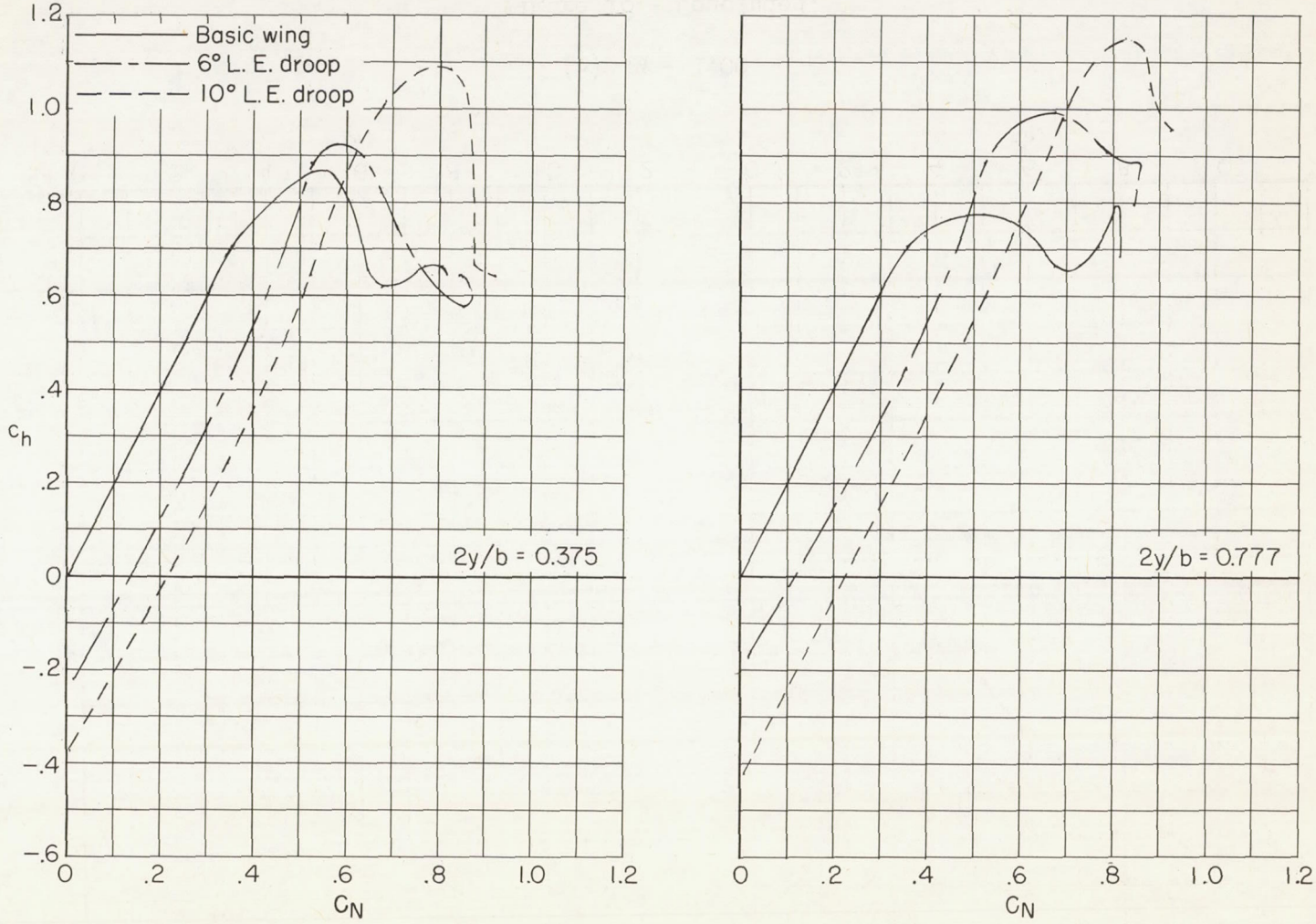
(b) M = 0.90.

Figure 18.- Continued.



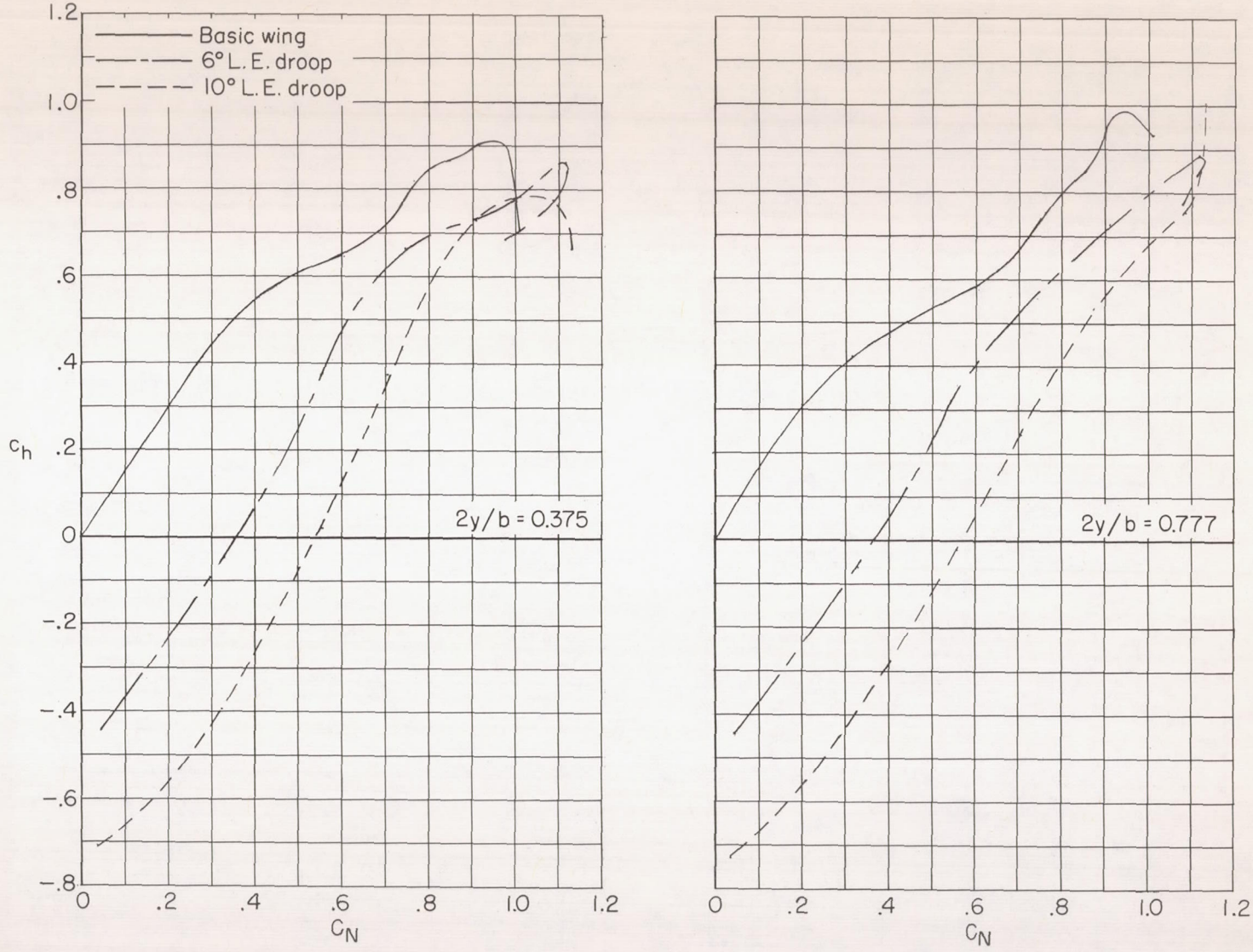
(c) M = 1.00.

Figure 18.- Concluded.



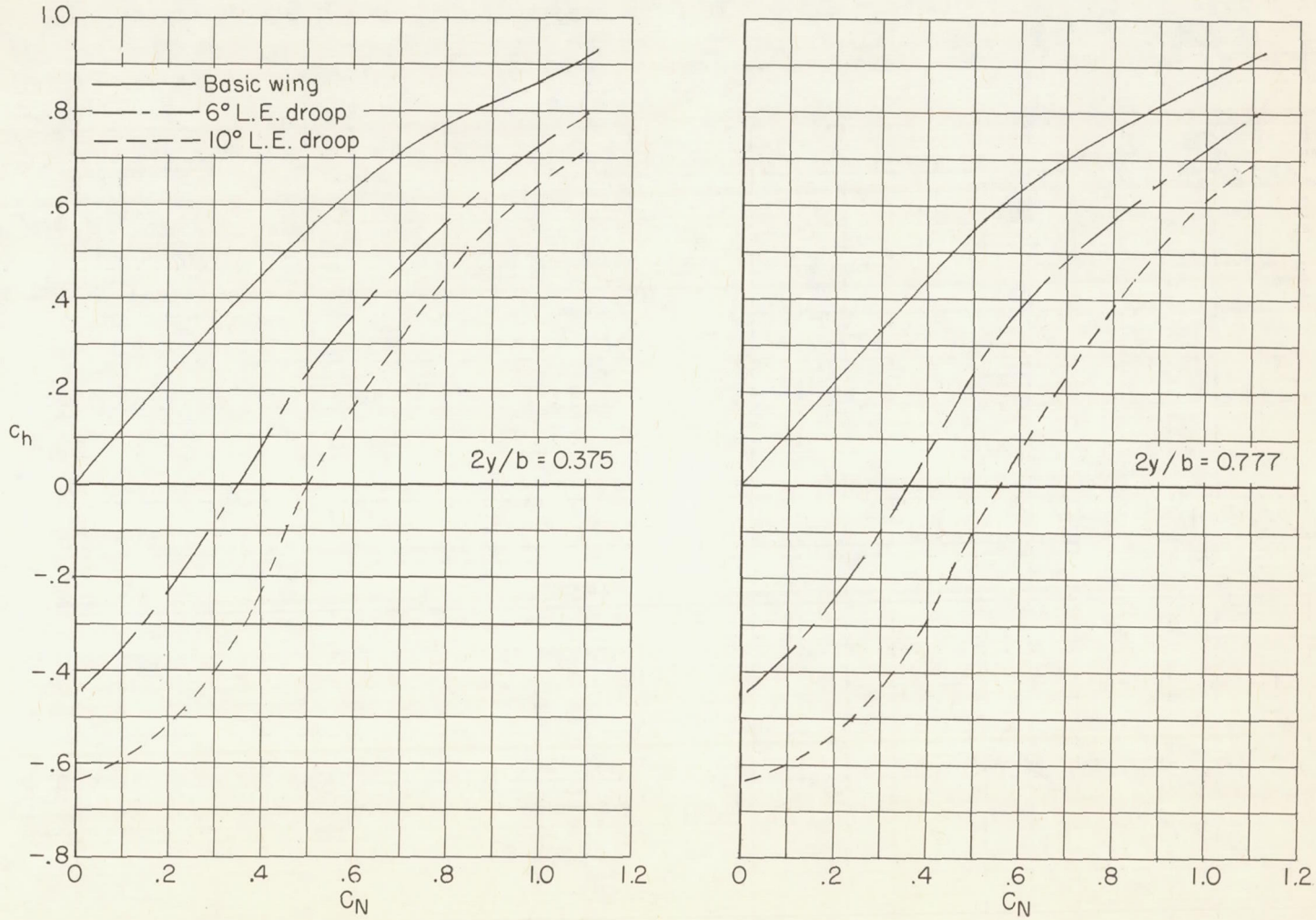
(a) M = 0.60.

Figure 19.- The effect of leading-edge droop on the section hinge-moment coefficient about 0.17c.



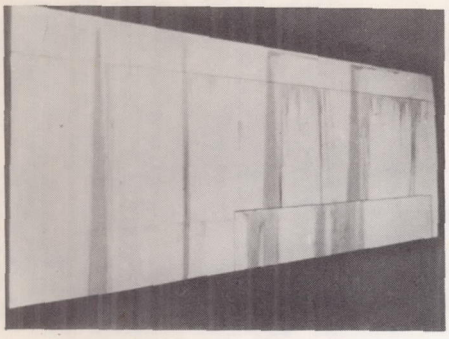
(b) M = 0.90.

Figure 19.- Continued.

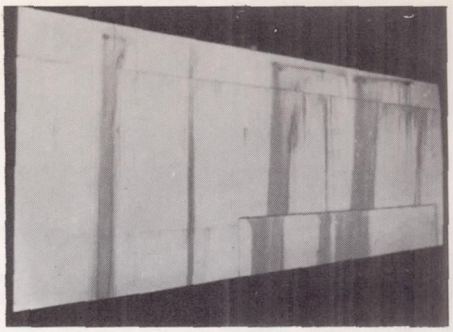


(c) M = 1.00.

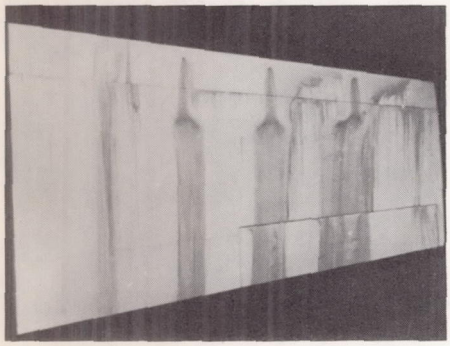
Figure 19.- Concluded.



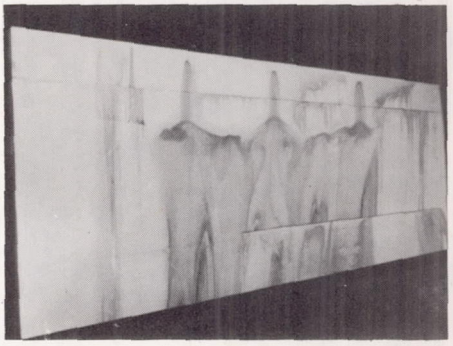
$\alpha = 2.0^{o}$



$\alpha = 2.6^{o}$



$\alpha = 5.0^{o}$



$\alpha = 6.7^{o}$



$\alpha = 9.3^{o}$



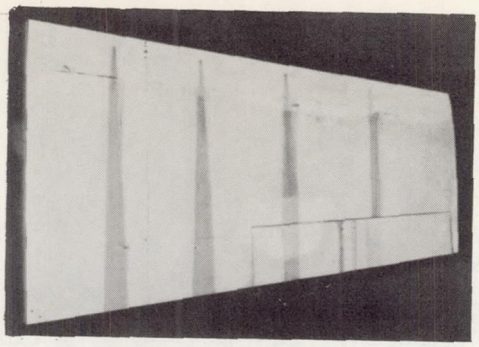
$\alpha = 13.4^{o}$

M = 0.80

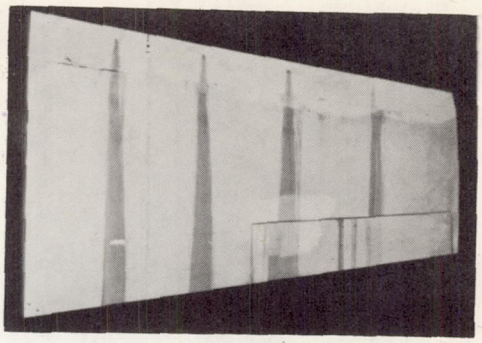
L-92430

(a) Basic wing.

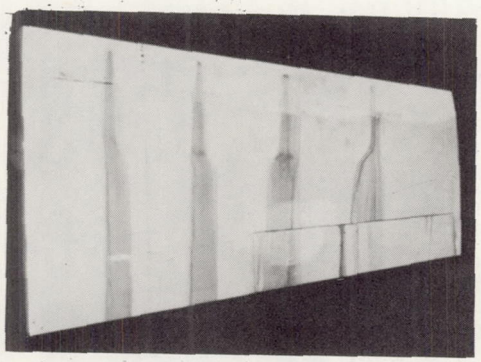
Figure 20.- Ink-flow photographs.



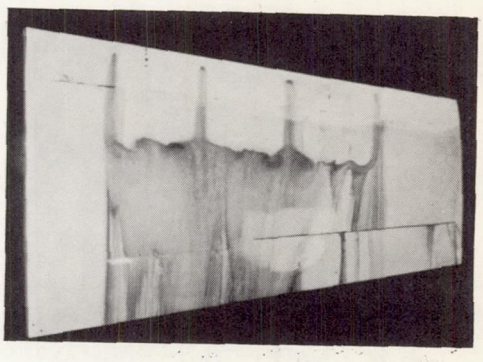
$\alpha = 0.6^{\circ}$



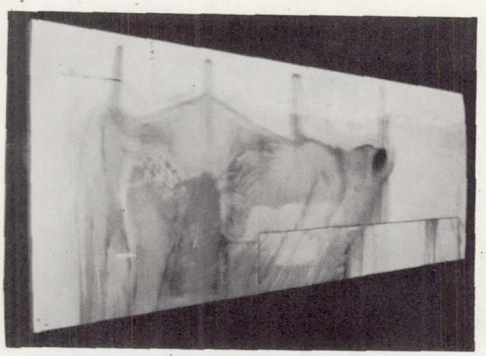
$\alpha = 2.3^{\circ}$



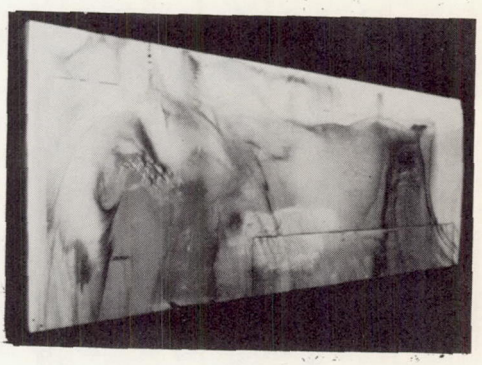
$\alpha = 5.2^{\circ}$



$\alpha = 7.0^{\circ}$



$\alpha = 9.2^{\circ}$



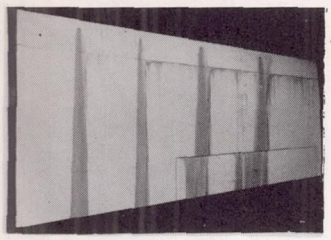
$\alpha = 13.7^{\circ}$

M = 0.80

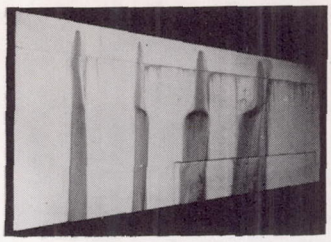
L-92431

(b) 6° L.E. droop.

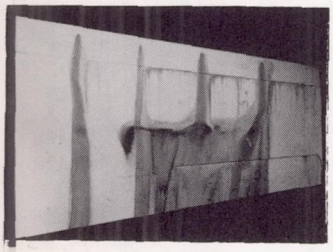
Figure 20.- Continued.



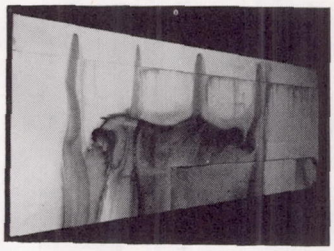
$\alpha = 2.7^{o}$



$\alpha = 4.5^{o}$



$\alpha = 5.7^{o}$



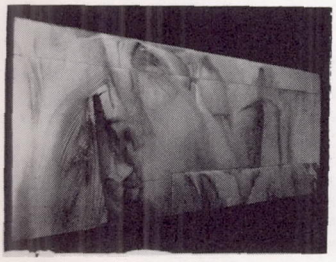
$\alpha = 7.4^{o}$



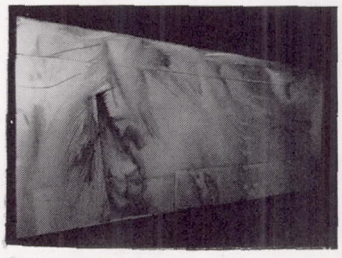
$\alpha = 9.4^{o}$



$\alpha = 10.5^{o}$



$\alpha = 11.5^{o}$



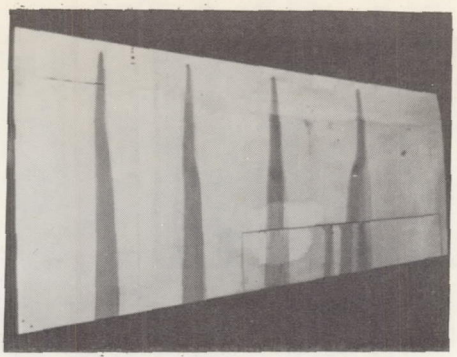
$\alpha = 16.6^{o}$

M = 0.85

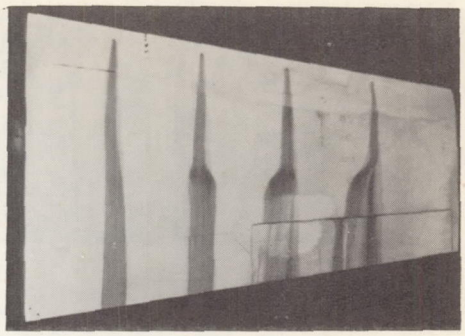
L-92432

(c) Basic wing.

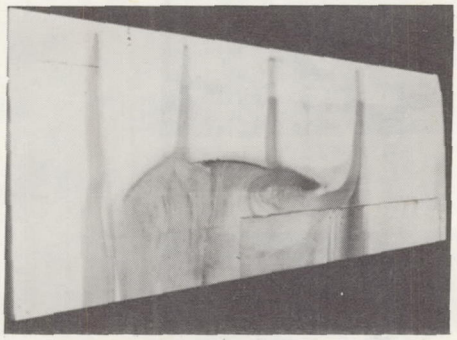
Figure 20.- Continued.



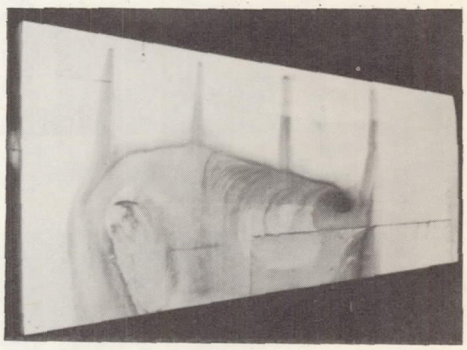
$\alpha = 2.3^{o}$



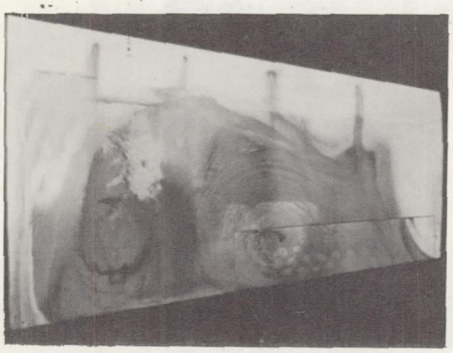
$\alpha = 5.2^{o}$



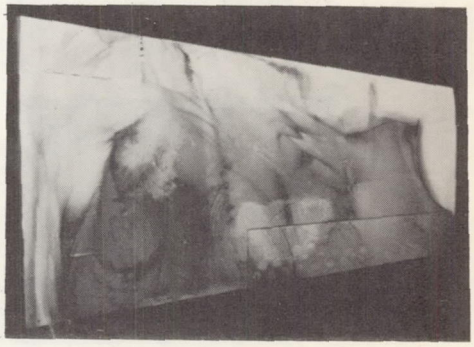
$\alpha = 6.4^{o}$



$\alpha = 7.6^{o}$



$\alpha = 10.3^{o}$



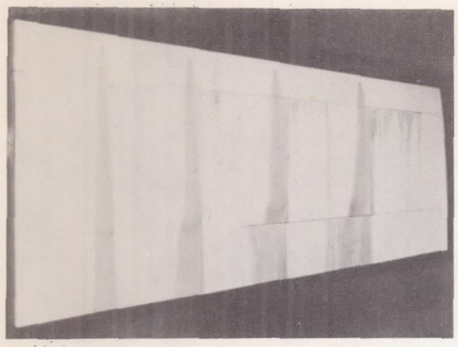
$\alpha = 13.7^{o}$

M = 0.85

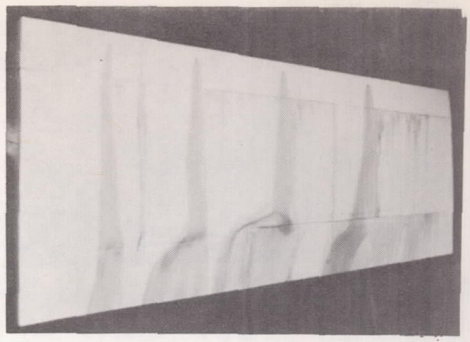
L-92433

(d) 6° L.E. droop.

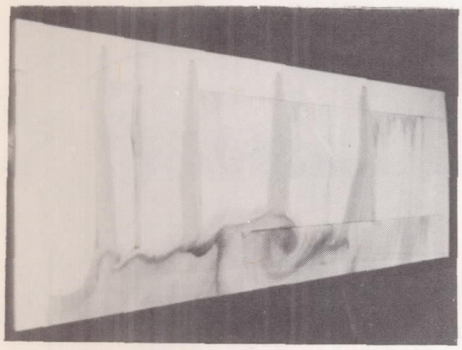
Figure 20.- Continued.



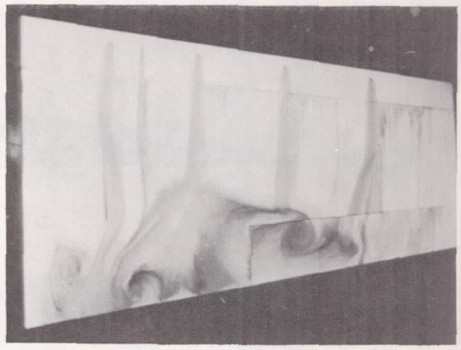
$\alpha = 2.8^{o}$



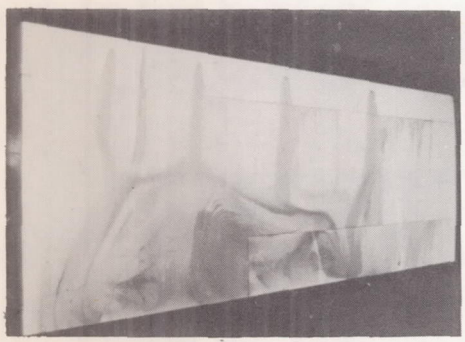
$\alpha = 4.7^{o}$



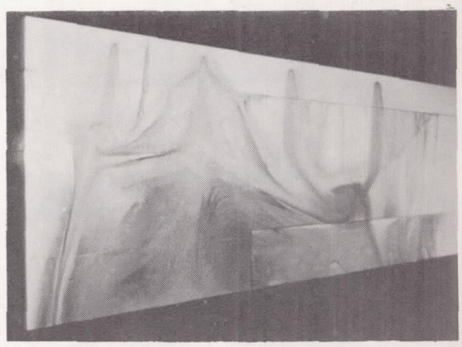
$\alpha = 5.9^{o}$



$\alpha = 7.5^{o}$



$\alpha = 9.7^{o}$



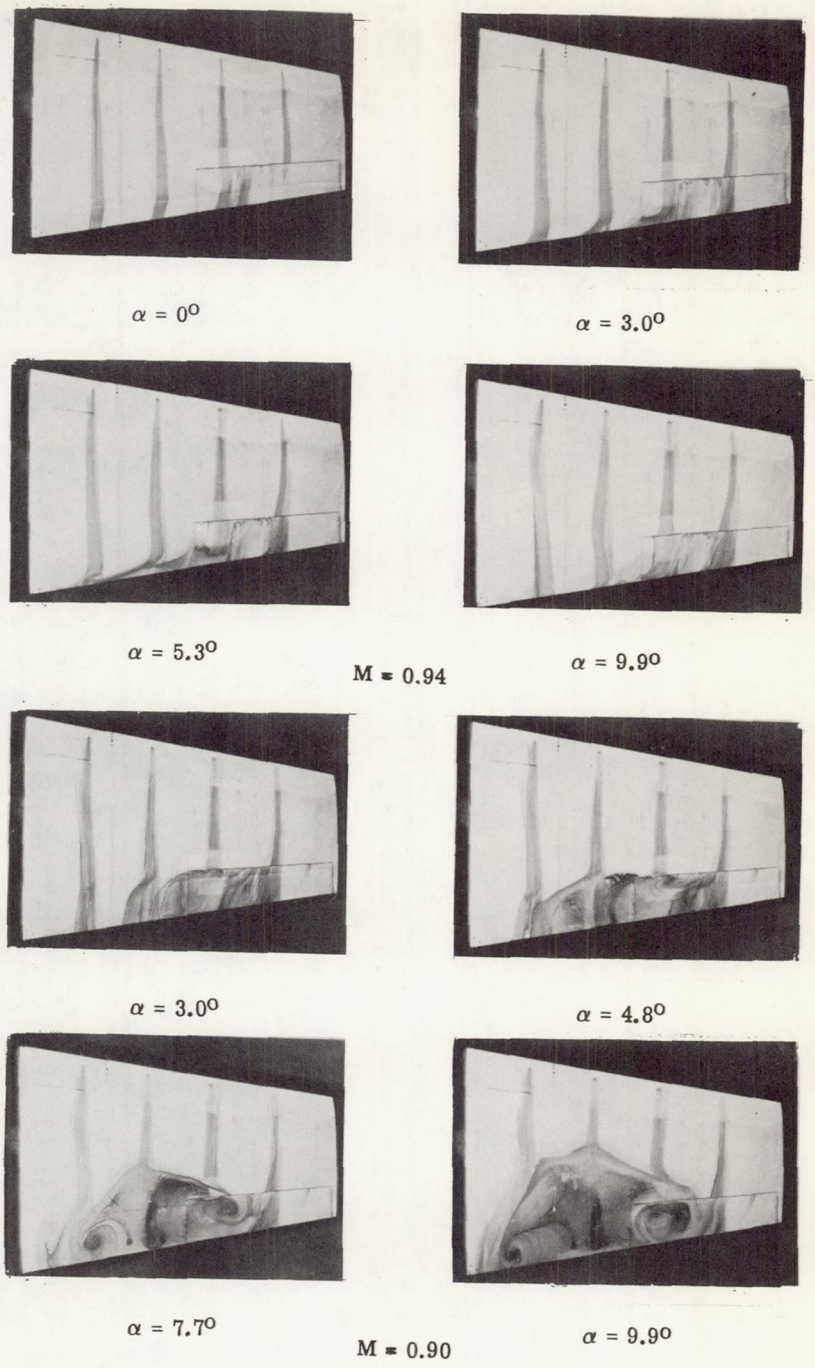
$\alpha = 12.8^{o}$

$M = 0.90$

L-92434

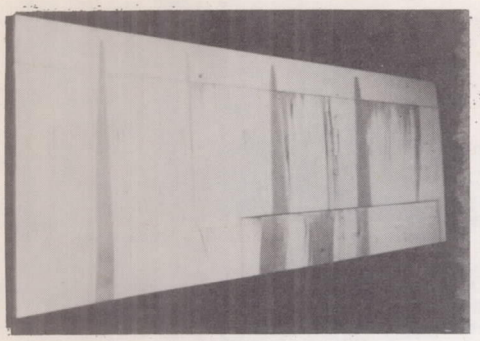
(e) Basic wing

Figure 20.- Continued.

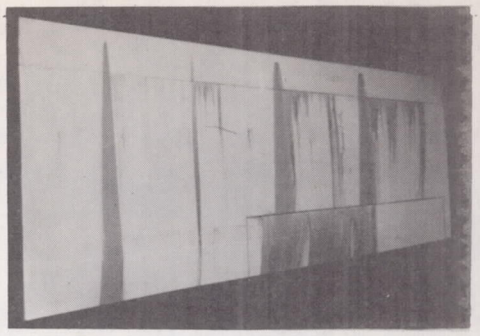


(f) 6° L.E. droop. L-92435

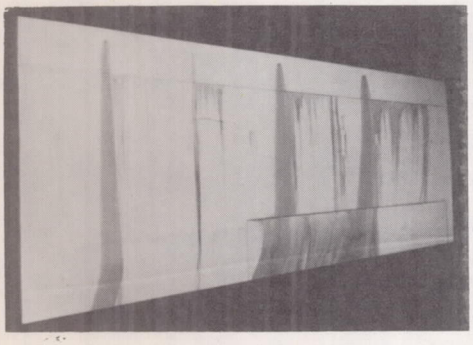
Figure 20.- Continued.



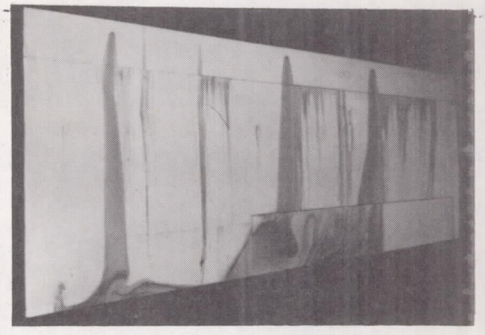
$\alpha = 0.3^{o}$



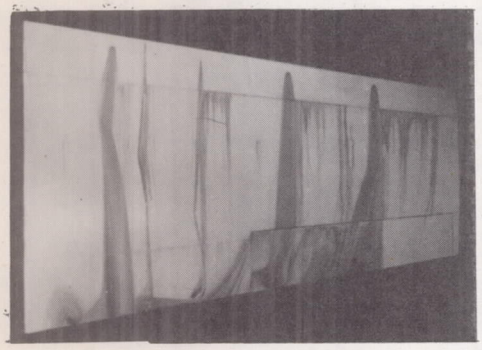
$\alpha = 1.6^{o}$



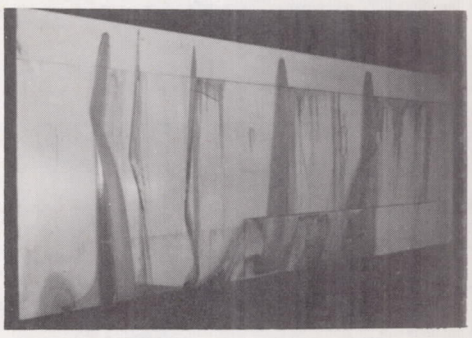
$\alpha = 2.8^{o}$



$\alpha = 5.2^{o}$



$\alpha = 8.1^{o}$



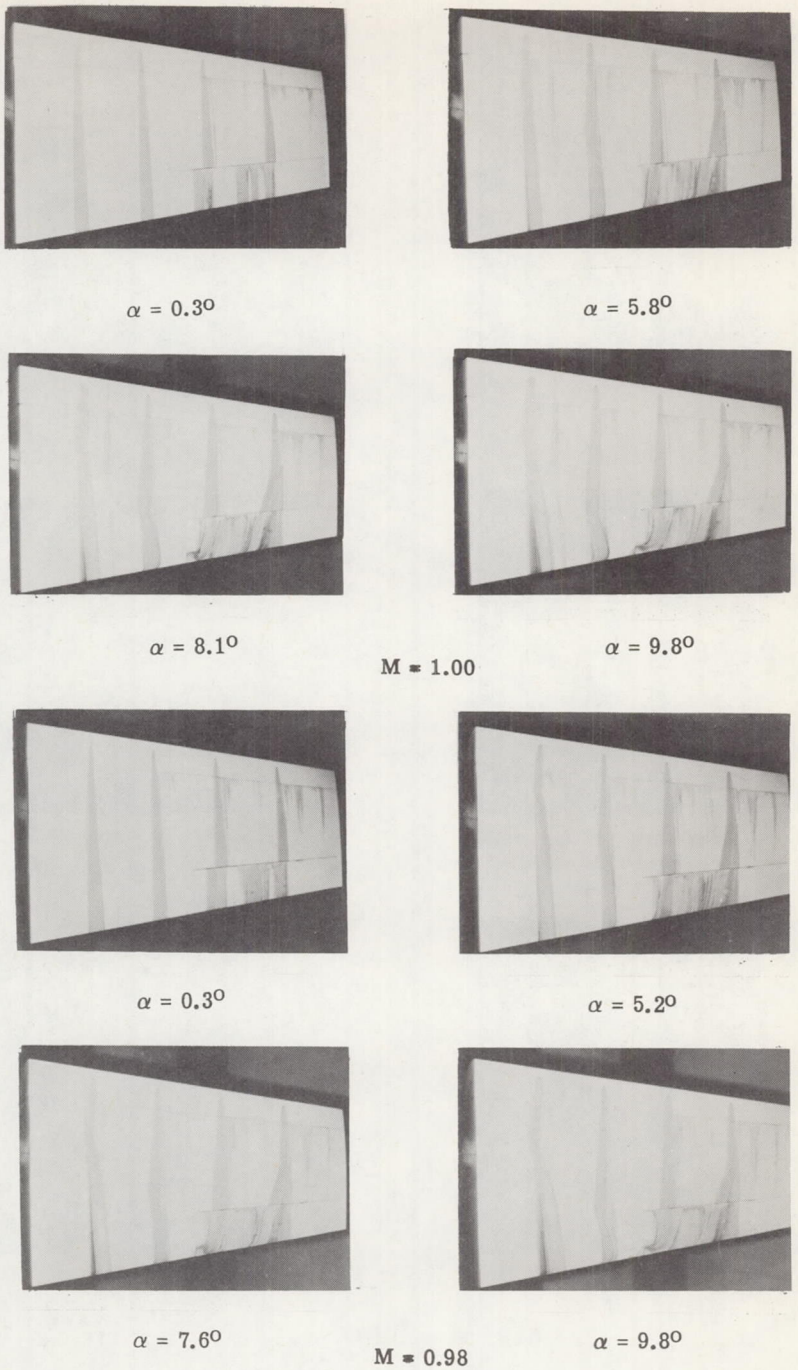
$\alpha = 9.8^{o}$

M = 0.94

L-92436

(g) Basic wing.

Figure 20.- Continued.



(h) Basic wing.

L-92437

Figure 20.- Concluded.